UNIVERSIDADE DE SÃO PAULO
FACULDADE DE MEDICINA DE RIBEIRÃO PRETO
PROGRAMA DE PÓS GRADUAÇÃO EM ONCOLOGIA CLÍNICA, CÉLULAS TRONCO E TERAPIA CELULAR

JESSICA RODRIGUES PLAÇA

Avaliação de perfis moleculares e microambientes em linfomas de células B

Ribeirão Preto

2022

JESSICA RODRIGUES PLAÇA

Avaliação de perfis moleculares e microambientes em linfomas de células B

Versão Original

Tese apresentada ao Programa de Pós-Graduação em Oncologia Clínica, Células Tronco e Terapia Celular da Faculdade de Medicina de Ribeirão Preto, Universidade de São Paulo para obtenção do título de Doutor em Ciências.

Área de Concentração: Diferenciação Celular Normal e Neoplásicas

Orientador: Prof. Dr. Wilson Araújo da Silva Jr.

Ribeirão Preto
2022

Rodrigues Plaça, Jessica

Avaliação de perfis moleculares e microambientes em linfomas de células B. / Jessica Rodrigues Plaça; orientador, Wilson Araujo da Silva Junior. – 2022.

69f.:il; 30 cm

Tese (Doutorado em Ciências) - Programa de Pós-Graduação em Oncologia Clínica, Células Tronco e Terapia Celular, Faculdade de Medicina de Ribeirão Preto, Universidade de São Paulo, Ribeirão Preto, 2022. Área de concentração: Diferenciação Celular Normal e Neoplásicas;

Orientador: Araujo da Silva Junior, Wilson

1. Linfoma de células B. 2. Bioinformática. 3. Perfil de expressão gênica.

Nome: PLAÇA, Jessica Rodrigues

Título: Avaliação de perfis moleculares e microambientes em linfomas de células B.

Tese apresentada à Faculdade de Medicina de Ribeirão Preto da Universidade de São Paulo, para obtenção do título de Doutor em Ciências

Aprovada em: _____/_____/_____

Banca examinadora

Dr(a):_____

Instituição:_____

Julgamento:_____

Assinatura:_____

Dr(a):_____

Instituição:_____

Julgamento:_____

Assinatura:_____

Dr(a):_____

Instituição:_____

Julgamento:_____

Assinatura:_____

Dr(a):_____

Instituição:_____

Julgamento:_____

Assinatura:_____

AGRADECIMENTOS

Ao Programa de Oncologia Clínica Células Tronco e Terapia Celular da FMRP, à Fundação Hemocentro da FMRP, aos órgãos de fomento Coordenação de Aperfeiçoamento de Pessoal de Nível Superior (Capes) , Conselho Nacional de Pesquisa (CNPq), à Fundação de Amparo à Pesquisa do Estado de São Paulo (FAPESP) e à Fundação de Apoio ao Ensino, Pesquisa e Assistência (FAEPA) do Hospital das Clínicas da Faculdade de Medicina de Ribeirão Preto por toda infra-estrutura, auxílio administrativo e financeiro a mim concedido.

À secretária do programa de pós-graduação em Oncologia Clínica, Células-Tronco e Terapia Celular da Faculdade de Medicina de Ribeirão Preto (FMRP), Rosana e Silvia, que sempre foi muito prestativas e não mediram esforços para me ajudar em processos administrativos.

Ao meu orientador, Prof. Dr. Wilson Araújo da Silva Jr, à Prof. Dra. Anke van den Berg, ao Prof. Dr. Marcel Nijland e ao Prof. Dr. Adjan Diepstra pela orientação, oportunidades de pesquisa e desenvolvimento do pensamento científico.

Aos colegas do Laboratório de Genética Molecular e Bioinformática (LGMB), pelas ótimas discussões científicas, convivência e boas risadas.

Aos meus pais, Agostinho e Lucia, principalmente por me darem amor incondicional. Vocês sempre me apoiam em meus ideais, me ajudam a tomar decisões de forma consciente e nunca mediram esforços para tornar meus sonhos possíveis. Sou eternamente grata à vocês.

Aos meus irmãos, Desirée e Alex, companheiros de uma vida e que hoje me inspiram à ser uma pessoa melhor.

Ao meu noivo Lucas por todo amor e cumplicidade que compartilha comigo todos os dias. Você fornece apoio fundamental aos meus objetivos e sou eternamente grata por todo cuidado e carinho que você tem comigo.

RESUMO

PLAÇA, Jessica Rodrigues. **Avaliação de perfis moleculares e microambientes em linfomas de células B.** 2022. Tese (Doutorado em Ciências) – Faculdade de Medicina de Ribeirão Preto, Ribeirão Preto, 2022.

O linfoma de células B compreende um grupo heterogêneo de tumores que surgem a partir de diferentes estágios de desenvolvimento das células B e do seu microambiente celular, retratando características morfológicas distintas. Vários estudos mostraram subgrupos biológicos importantes, que muitas vezes coincidem com resposta à terapia. No entanto, a maioria desses estudos não foram validados em coortes independentes ou os dados disponíveis são escassos. Assim, o objetivo deste projeto foi identificar os genes associados as assinaturas específicas de linfoma (relacionadas ao tumor e ao microambiente), caracterizar seus perfis de expressão e associar esses perfis à funções biológicas e desfechos clínicos. Caracterizamos padrões de expressão gênica de dois subtipos de linfomas de células B. O primeiro foi o linfoma de Hodgkin clássico (LHc) que possui células T CD4+ altamente abundantes nas proximidades das células tumorais, consideradas essenciais para a sobrevivência das células tumorais, mas são mal definidas. Embora sejam ativadas, elas podem não expressar o marcador de ativação CD26. Assim, comparamos suspensões de células T de linfonodo CD4+CD26- e CD4+CD26+ por RNA-seq que revelou que as células T CD4+CD26- foram apresentadas à antígenos provavelmente pela expressão de fatores de transcrição associados à exaustão TOX e TOX2, *checkpoints* imunológicos PDCD1 e CD200 e quimiocina CXCL13, que estavam entre os 100 genes significativamente enriquecidos em comparação com as células T CD4+CD26+. Esta população é provavelmente um dos principais contribuintes para as taxas de resposta muito altas aos inibidores de *checkpoint* imunológico em LHc. O segundo grupo foi o linfoma difuso de grandes células B (LDGCB), onde além do classificador de células de origem (CO), nenhuma assinatura foi reproduzida em estudos independentes ou avaliada para capturar aspectos distintos da biologia de LDGCB. Assim, reproduzimos 4 assinaturas em 175 amostras da corte HOVON-84 em um painel de 117 genes usando a plataforma NanoString. As quatro

assinaturas de genes capturam a CO, a atividade do gene MYC, a sinalização do receptor da célula B, a fosforilação oxidativa e a resposta imune. O desempenho de nossos algoritmos de classificação foi confirmado nos conjuntos de dados originais. Conseguimos validar três das quatro assinaturas. O algoritmo CO resultou em 94 (54%) casos relacionados à células B do centro germinativo (CGB), 58 (33%) de células B ativadas (CBA) e 23 (13%) casos não classificados. O classificador MYC revelou 77 casos associados ao escore de alta atividade MYC (44%) e essa assinatura foi observada com mais frequência no ABC em comparação ao GCB LDGCB (68% vs. 32%, $p < 0,00001$). A assinatura da resposta do hospedeiro (RH) do agrupamento consenso estava presente em 55 (31%) pacientes, enquanto os demais agrupamentos não puderam ser reproduzidos. A sobreposição entre CO, grupo consenso e atividade de MYC diferenciou seis clusters de expressão gênica: CGB/MYC-alto (12%), CGB/RH (16%), CGB/não-RH (27%), CO-não classificado (13%) %), CBA/MYC-alto (25%) e CBA/MYC-baixo (7%). Em conclusão, este estudo identificou novos alvos moleculares acionáveis para subgrupos específicos de pacientes, o que pode ajudar no desenvolvimento de estratégias terapêuticas mais precisas e eficazes do linfoma de células B no futuro.

Palavras-chave: Linfoma de células B. Bioinformática. Perfil de expressão gênica.

ABSTRACT

PLAÇA, Jessica Rodrigues. **Evaluation of molecular profiles and micro-environments in B-cell lymphomas**. 2022. Tese (Doutorado em Ciências) – Faculdade de Medicina de Ribeirão Preto, Ribeirão Preto, 2022.

B-cell lymphoma comprises a heterogeneous group of malignancies that arise from a specific developmental stage of B-cells and shape of their microenvironment as depicted by the distinct morphological features. Several studies have shown biologically meaningful subgroups, which often coincides with either good or bad response to therapy. However, most of these studies have not been validated in independent cohorts and for several B-cell lymphoma subtypes available data are scarce. Thus, the aim of this project was to identify the genes associated with specific lymphoma signatures (either tumor related or microenvironment), characterize their expression profiles, and associate these profiles with biological functions and clinical outcomes. We characterized an in-depth gene expression pattern of two groups of B-cell lymphomas. The first was the classical Hodgkin lymphoma which has highly abundant CD4+ T cells in the vicinity of tumor cells are considered essential for tumor cell survival but are ill-defined. Although they are activated, they consistently lack expression of activation marker CD26. We compared sorted CD4+CD26- and CD4+CD26+ T cells lymph node cell suspensions by RNA sequencing. This revealed that CD4+CD26- T cells are antigen experienced. This can be explained by the expression of exhaustion associated transcription factors *TOX* and *TOX2*, immune checkpoints *PDCD1* and *CD200*, and chemokine *CXCL13*, which were amongst the 100 significantly enriched genes in comparison with the CD4+CD26+ T cells. This population is likely a main contributor to the very high response rates to immune checkpoint inhibitors in cHL. The second group was diffuse large B-cell lymphoma which multiple gene expression profiles have been identified but besides the cell of origin (COO) classifier, no signatures have been reproduced in independent studies or evaluated for capturing distinct aspects of DLBCL biology. So, we reproduced 4 signatures in 175 samples of the HOVON-84 trial on a panel of 117 genes using the NanoString platform. The four gene signatures capture the COO, MYC activity, B-cell receptor signaling,

oxidative phosphorylation, and immune response. Performance of our classification algorithms were confirmed in the original datasets. We were able to validate three of the four GEP signatures. The COO algorithm resulted in 94 (54%) germinal center B-cell (GCB) type, 58 (33%) activated B-cell (ABC) type, and 23 (13%) unclassified cases. The MYC-classifier revealed 77 cases with a high MYC-activity score (44%) and this MYC-high signature was observed more frequently in ABC as compared to GCB DLBCL (68% vs. 32%, $p < 0.00001$). The host response (HR) signature of the consensus clustering was present in 55 (31%) patients, while the B-cell receptor signaling, and oxidative phosphorylation clusters could not be reproduced. The overlap of COO, consensus cluster and MYC activity score differentiated six gene expression clusters: GCB/MYC-high (12%), GCB/HR (16%), GCB/non-HR (27%), COO-Unclassified (13%), ABC/MYC-high (25%), and ABC/MYC-low (7%). In conclusion, this study lead to identification of new actionable molecular targets for specific patient subgroups. This may help in the development of more precise and effective therapeutic strategies for B-cell lymphoma patients in the future.

Keywords: B-cell lymphoma. Bioinformatics. Gene expression profile

LISTA DE FIGURAS

LISTA DE TABELAS

SUMÁRIO

1 INTRODUCTION

Lymphomas mainly comprise Hodgkin lymphoma (HL) and non-Hodgkin lymphoma (NHL), representing a heterogeneous group of lymphoproliferative diseases. B-cell lymphomas account for almost 95% of all lymphoma cases and an annual incidence of around 20 new cases per 100,000 persons (IAFC, 2018). It is estimated that for each year of the triennium 2020/2022, 2.640 new cases of HL and 12030 new cases of NHL are diagnosed in Brazil (CÂNCER, 2020). While in the Netherlands, 500 HL and 3850 NHL cases were reported in 2018 (SWERDLOW; CAMPO; HARRIS, 2017).

Patients with B-cell lymphomas are usually characterized by lymphadenopathy, extranodal disease or both and present the potential for multiple organ involvement (SEHN; SALLES, 2021). Despite improvement of treatment strategies, the number of lymphoma-associated deaths remains high with 5-year survival rates varying between 30-90% depending on stage and lymphoma subtype. In addition, undesired treatment-induced side effects, such as cardiac disease, secondary malignancies and infertility present major risks for lymphoma patients (SWERDLOW; CAMPO; HARRIS, 2017).

Despite successful introduction of novel agents in indolent lymphoma and substantial increase in biological understanding in specific B-cell lymphoma subtypes, attempts to improve survival by combining standard therapy with novel targeted agents yielded disappointing results for some aggressive B-cell lymphomas, like the common Diffuse large B-cell lymphoma (DLBCL) (SWERDLOW; CAMPO; HARRIS, 2017). At the same time, although survival in young patients with HL is favorable, the outcome of patients above the age of 60 years is still poor. One barrier to the effective use of novel therapies targeting specific pathways is the biological intra- and inter-individual heterogeneity of B-cell lymphoma and the likely existence of multiple distinct subtypes, which might respond differentially to specific treatments. To permit more accurate targeting in clinical trials, it is essential to define distinct molecular subtypes between patients and assess heterogeneity within patients, permitting stratification between patients that are likely to respond to standard treatment and patients that may benefit from emerging therapies.

Large-scale molecular characterization studies in combination with advanced bioinformatics approaches to identify new molecular subgroups with clinical utility, should be implemented in clinical practice to maximize treatment of the patients, improving

outcome, selecting candidates for escalation therapy, and ultimately also de-escalation studies.

1.1 Tumor microenvironment

The tumor microenvironment (TME) is a complex network that comprises cellular and noncellular components, forming a physical barrier around tumor cells (CASEY; AMEDEI; AQUILANO; AZMI *et al.*, 2015). Accumulating studies have suggested that the TME components play important roles in the initiation and maintenance of carcinogenesis instead of being bystanders (WANG; DING; ZHENG; XIAO *et al.*, 2020). TME is instrumental in a variety of biological processes, including pathogenesis, progression, metastasis and drug resistance, through sustained proliferation and immune escape (HUI; CHEN, 2015). Given the limited efficacy of standard therapies in several patients, TME-based therapies have been explored as new treatment strategies to achieve a more immunogenic environment and better drug delivery, ultimately increasing the response rates of patients. Recent studies suggest that the composition of TME is essential for the pathogenesis of lymphoma. Moreover, the TME also provides new strategies for targeted therapies and tumor prognosis prediction.

The TME can be divided into two parts: the immune microenvironment that contains immune cells and the nonimmune microenvironment dominated by fibroblasts (JUNTTILA; DE SAUVAGE, 2013). The immune microenvironment consists of T and B lymphocytes, tumor-associated macrophages (TAMs), myeloid-derived suppressor cells (MDSCs), tumor-associated neutrophils (TANs), natural killer (NK) cells, dendritic cells (DCs) and others. These cells mediate the immunosuppressive microenvironment and escape immunity. The nonimmune microenvironment mainly consists of stromal cells, including cancer-associated fibroblasts (CAFs), extracellular matrix (ECM), pericytes, mesenchymal stromal cells and other secreted molecules, including growth factors, cytokines, chemokines and extracellular vesicles (BEJARANO; JORDĀO; JOYCE, 2021).

1.3 Classical Hodgkin lymphoma

Hodgkin lymphoma (HL) is a B-cell malignancy that has a bi-modal age distribution with a peak in young adults (age 20–34) and in elderly patients (age 65-77). Especially elderly patients still have a poor outcome. Whether this is due to intrinsic differences in

tumor and TME or are related to the toxicity of treatment in elderly patients is unknown. HL can be subdivided into classical HL (cHL) and nodular lymphocyte predominant HL (NLPHL) based on morphological and clinical differences (SWERDLOW; CAMPO; HARRIS, 2017; SWERDLOW; CAMPO; PILERI; HARRIS *et al.*, 2016). NLPHL is more frequent in the youngest patients with mediastinal involvement and sometimes bulky disease. Differential diagnosis is with primary mediastinal lymphoma CD20+, CD23+, or CD30+ occurring in young women or in patients with rare grey-zone lymphomas.

cHL is characterized by a low number of tumor cells, called Hodgkin-Reed Sternberg (HRS) cells which derive from germinal centre B-cells, surrounded by a heterogeneous inflammatory infiltrate (NAGASAKI; TOGASHI; SUGAWARA; ITAMI *et al.*, 2020; POPPEMA; BHAN; REINHERZ; POSNER *et al.*, 1982). HRS cells evade anti-tumor immune responses by shaping the TME and by inhibiting immune cells (CADER; SCHACKMANN; HU; WIENAND *et al.*, 2018; HOLLANDER; ROSTGAARD; SMEDBY; MOLIN *et al.*, 2018; LIU; SATTARZADEH; DIEPSTRA; VISSER *et al.*, 2014). The highly abundant CD4+ T cells also play a critical role in the pathogenesis of cHL. CD4+ T cells are actively recruited by the HRS cells and can form so-called rosettes in a subset of cases (IELLEM; MARIANI; LANG; RECALDE *et al.*, 2001; ISHIDA; ISHII; INAGAKI; YANO *et al.*, 2006; NIENS; VISSER; NOLTE; VAN DER STEEGE *et al.*, 2008; POPPEMA; BHAN; REINHERZ; POSNER *et al.*, 1982; STUART; WILLIAMS; HABESHAW, 1977). In each rosette, the CD4+ T cells physically interact with an HRS cell, providing it with pro-survival signals and shielding it from cytotoxic CD8+ T cells and NK cells (LIU; SATTARZADEH; DIEPSTRA; VISSER *et al.*, 2014). Recently, was shown that rosetting CD4+ T cells communicate with the HRS cell through formation of the immunological synapse, with a central role for HLA class II-T cell receptor (TCR) interactions (VELDMAN; VISSER; HUBERTS-KREGEL; MULLER *et al.*, 2020). In addition, CD4+ T cells have been implicated as key players in the response to programmed cell death-1 (PD-1) immune checkpoint inhibition. Membranous HLA class II expression by HRS cells was predictive for complete remission and increased progression-free survival (ROEMER; REDD; CADER; PAK *et al.*, 2018). Moreover, CD4+ TCR diversity significantly increased in the blood of patients who achieved complete remission after PD-1 inhibition (CADER; HU; GOH; WIENAND *et al.*, 2020).

Thus, CD4+ T cells residing in proximity to HRS cells are emerging as crucial players in cHL pathogenesis and response to PD-1 blockade.

In recent years, studies on the characterization of the cHL TME have suggested that the CD4+ T cells are mainly CD4+ regulatory T cells (Tregs) and exhausted T-effector cells (AOKI; CHONG; TAKATA; MILNE *et al.*, 2020; CADER; SCHACKMANN; HU; WIENAND *et al.*, 2018). Exhausted T cells are characterized by increased expression of inhibitory cell surface receptors, reduced secretion of cytokines, reduced cytotoxicity and reduced proliferative potential. Indeed, expression of immune checkpoint molecules PD-1, CTLA-4 and/or LAG-3 has been identified in variable proportions of cHL CD4+ T cells (AOKI; CHONG; TAKATA; MILNE *et al.*, 2020; CAREY; GUSENLEITNER; LIPSCHITZ; ROEMER *et al.*, 2017; PATEL; WEIRATHER; LIPSCHITZ; LAKO *et al.*, 2019). However, detailed and unbiased characterization of CD4+ T cells in the cHL TME has remained challenging due to the difficulty of separating CD4+ T cells in proximity to HRS cells from more distant CD4+ T cells in lymph nodes (FROMM; KUSSICK; WOOD, 2006). The CD4+ T cells close to the HRS cells are known to express several activation-associated cell surface markers, including CD38 and CD69, but not CD26, while CD4+ T cells more distant from HRS cells do express CD26 (MA; VISSER; BLOKZIJL; HARMS *et al.*, 2008; POPPEMA, 1989; 1996; TANAKA; CAMERINI; SEED; TORIMOTO *et al.*, 1992). CD26, also known as dipeptidyl peptidase IV (DPP4), is a proteolytic enzyme that is upregulated after stimulation under normal physiological conditions and plays a role in co-stimulation (FLEISCHER, 1994; KLEMANN; WAGNER; STEPHAN; VON HÖRSTEN, 2016). However, CD4+CD26- T cells in cHL remain CD26 negative after activation and can also not or only moderately induce expression of T cell activation-associated cytokines, suggesting a functionally unresponsive or anergic state (MA; VISSER; BLOKZIJL; HARMS *et al.*, 2008; POPPEMA, 1989; 1996; TANAKA; CAMERINI; SEED; TORIMOTO *et al.*, 1992). Moreover, the CD4+CD26- T cell population expresses more Treg and Th17 cell associated markers compared to CD4+ CD26+ T cells (MA; VISSER; BLOKZIJL; HARMS *et al.*, 2008).

1.2 Diffuse large B-cell lymphoma

DLBCL, not otherwise specified (NOS) is a heterogeneous disease that accounts for 40% of all B-NHL lymphomas (SWERDLOW; CAMPO; HARRIS, 2017). The outcome of patients with a good risk disease as determined by the clinical International Prognostic Index (IPI) score is excellent using chemoimmunotherapy regimens based on the combination of anthracyclines and anti-CD20 antibodies, i.e. R-CHOP (rituximab, cyclophosphamide, doxorubicin, vincristine and prednisone) (SEHN; BERRY; CHHANABHAI; FITZGERALD *et al.*, 2007). However, in high risk patients nearly 40% of patients fail R-CHOP. These patients suffer from recurrent or progressive disease that is often fatal. DLBCL displays distinct clinical, histological and immunophenotypic features, with a highly variable short-term and long-term response to treatment making the identification and characterization of this B-NHL a major priority (SWERDLOW; CAMPO; HARRIS, 2017).

The past 20 years the biological basis of DLBCL has been extensively studied mainly by gene expression profiling (GEP), fluorescence in situ hybridization (FISH) and next generation sequencing (NGS) for identification of DLBCL biological subgroups which can guide the clinical procedure. The cell-of-origin (COO) concept was first published in 2000, dividing DLBCL based on GEP profiles in germinal center B-cell (GCB) type, activated B-cell (ABC) type and unclassified cases (15%) (ALIZADEH; EISEN; DAVIS; MA *et al.*, 2000). The COO subgroups were shown to have distinct features indicating involvement of different oncogenic pathways. Patients with ABC-type DLBCL showed an inferior outcome in a retrospective setting (ALIZADEH; EISEN; DAVIS; MA *et al.*, 2000). So far, clinical studies targeted towards specific oncogenetic characteristics of ABC-type DLBCL patients, e.g., combining the small molecules bortezomib, ibrutinib, and lenalidomide to R-CHOP have not been successful to improve outcome, which underpins that a simple dichotomy to define DLBCL does not sufficiently capture the oncogenetic complexity of this disease (LEONARD; KOLIBABA; REEVES; TULPULE *et al.*, 2017; VITOLO; WITZIG; GASCOYNE; SCOTT *et al.*, 2019; YOUNES; SEHN; JOHNSON; ZINZANI *et al.*, 2019). Moreover, about 15% of DLBCL cases remain unclassified and these cases do not have other characteristic aberrations that can advise the treatment of these patients (ALIZADEH; EISEN; DAVIS; MA *et al.*, 2000).

In 2017 the World Health Organization (WHO) classification categorized high grade B-cell lymphomas with a MYC rearrangement in combination with a BCL2 and/or BCL6 rearrangements as a separate entity, called high grade B cell lymphoma with a double hit (HGBCL DH) (SWERDLOW; CAMPO; HARRIS, 2017). Within this group of HGBCL DH lymphomas, especially those cases with a MYC-IG rearrangement have an inferior survival (ROSENWALD; BENS; ADVANI; BARRANS *et al.*, 2019). Despite the use of more intensive chemotherapy and small molecules within this subgroup no improvement in outcome has been achieved in randomized clinical trials (CASAN; BARRACLOUGH; SHORTT; HAWKES, 2019; CHAMULEAU; BURGGRAAFF; NIJLAND; BAKUNINA *et al.*, 2019).

Traditionally, DLBCL had been recognized as less dependent on its microenvironment as compared to other lymphomas, in agreement with a near-complete disorganization and/or displacement of normal lymphoid architecture. In addition, given that tumors with very distinct genetic backgrounds share similar TME composition, this should not form the sole basis of a comprehensive taxonomy. However, there is increasing evidence that an immunologic niche and cross-talk with various immune cell types is critical for disease development and adds another layer of complexity to genetic and molecular subtypes. In particular, it has been increasingly recognized that the disrupted cross-talk between lymphoma cells and the microenvironment contributes to the ability of lymphoma cells to escape the immune surveillance of the host in DLBCL (SCOTT; GASCOYNE, 2014).

From 2010 onward, the focus has been in deciphering the mutational landscape of DLBCL (CHAPUY; STEWART; DUNFORD; KIM *et al.*, 2018; LACY; BARRANS; BEER; PAINTER *et al.*, 2020; REDDY; ZHANG; DAVIS; MOFFITT *et al.*, 2017; SCHMITZ; WRIGHT; HUANG; JOHNSON *et al.*, 2018). The established mutational profiles show overlapping features and are at least partially correlated to COO, but not to MYC rearrangements (CHAPUY; STEWART; DUNFORD; KIM *et al.*, 2018). Identifying genetic abnormalities that drive the disease in a group of patients can help identify the best drug for treatment. However, due to the diversity of DLBCL-causing drivers and intra-individual tumor heterogeneity multiple drugs might be needed to effectively treat patients. Identifying homogeneous subgroups may help to more accurately establish optimal

treatment regimens. Moreover, identification of main drivers of lymphomagenesis, no matter which lymphoma-initiating event caused the lymphoma, may allow development of novel targeted treatment strategies.

In parallel several GEP studies have identified biological subgroups that further subclassify DLBCL (CAREY; GUSENLEITNER; CHAPUY; KOVACH *et al.*, 2015; CHAN; TELENIUS; HEALY; BEN-NERIAH *et al.*, 2015; CIAVARELLA; VEGLIANTE; FABBRI; DE SUMMA *et al.*, 2018; ENNISHI; JIANG; BOYLE; COLLINGE *et al.*, 2019; KEANE; VARI; HERTZBERG; CAO *et al.*, 2015; LENZ; WRIGHT; DAVE; XIAO *et al.*, 2008; LI; KIM; RAI; BOLLA *et al.*, 2009; MASQUÉ-SOLER; SZCZEPANOWSKI; KOHLER; SPANG *et al.*, 2013; MONTI; SAVAGE; KUTOK; FEUERHAKE *et al.*, 2005; ROSENWALD; BENS; ADVANI; BARRANS *et al.*, 2019; SCOTT; WRIGHT; WILLIAMS; LIH *et al.*, 2014; SHIPP; ROSS; TAMAYO; WENG *et al.*, 2002; STAIGER; ALTENBUCHINGER; ZIEPERT; KOHLER *et al.*, 2020). These studies have generated profiles related to tumor cell characteristics including MYC activity and composition of the TME. However, the biological relevance and clinical impact of these gene signatures have not resulted in incorporation in clinical trials, probably due to the lack of validation cohorts.

2 AIM

2.1 Overall aim

The overall aim of this project is to define gene expression signatures to characterize molecular B cell lymphoma subgroups.

2.2 Specifics aims

A- Characterize gene expression profiles of rosetting T cells in classical HL

B- Verify the reproducibility of published gene expression signatures for DLBCL.

3 CHARACTERIZE GENE EXPRESSION PROFILES OF ROSETTING T CELLS IN CLASSICAL HL

This specific aim was to further characterize the CD4+CD26- T cells in the TME that are in the direct vicinity of the malignant HRS cells. We compared CD4+CD26- to CD4+CD26 + T cells sorted from cHL lymph node derived cell suspensions and characterized their gene expression profiles. We established differentially expressed gene signatures, most likely CD4+ T cell subset lineages.

3.1 Materials and methods

3.1.1 Patients, tissue, and cell suspensions

For bulk RNA-seq, cryopreserved cell suspensions derived from lymph nodes of 19 cHL patients were retrieved from the cell bank of the department of Pathology and Medical Biology, University Medical Center Groningen, Groningen, The Netherlands. Patient characteristics are summarized in Table 1.

Table 1. Patient Characteristics

Characteristic	***Number of samples (%)***
Median age (range)	38 (13-80)
Female	10 (53)
Histology	
NS	14 (74)
MC	2 (11)
LR	2 (11)
NOS	1 (5)
EBV positive	7 (37)
Relapse	4 (21)

Patients were selected based on membranous HLA class II positivity (>90%) on the HRS cells as determined by immunohistochemistry for HLA-DP, DQ, DR (clone: CR3/43; 1:200; Dako; Santa Clara, CA, USA) on corresponding formalin fixed paraffin embedded

(FFPE) tissue sections. Material was used in accordance with the ethical principles of the Declaration of Helsinki. The medical ethical review board of the UMCG approved the protocol under #RR202100080.

3.1.2 Cell sorting

All 19 cell suspensions were stained for CD4 (clone: Edu-2) and CD26 (clone: 2A6) as described previously (MA; VISSER; BLOKZIJL; HARMS *et al.*, 2008). CD4+CD26- and CD4+CD26+ T cells were sorted using a MoFlo sorter (BD Biosciences, CA, USA) with a 70 µm nozzle. Purity of sorted populations was checked and was at least 94% or higher for all 38 sorted populations.

3.1.3 RNA isolation and bulk RNA sequencing

Total RNA was extracted from the 38 populations using a miRNeasy Mini or Micro kit (Qiagen; Hilden, Germany) according to manufacturer's instructions. The concentration and quality of total RNA was determined using a Fragment Analyzer and all samples had an RNA integrity number of 8.5 or above. Three of the 38 populations, all CD4+CD26+, were excluded from RNA-seq due to an insufficient amount of RNA (<10 ng total). RNA libraries were made after depletion of rRNA (rRNA depletion kit, NEB #E6310) using the NEBNext Ultra II Directional RNA library prep kit for Illumina at GenomeScan (Leiden, The Netherlands) according to manufacturer's instructions (NEB #E7760S/L). Paired-end sequencing with a read length of 151 nucleotides was performed on an Illumina NovaSeq6000 sequencer (Illumina; CA, USA) aiming at ~25 million paired reads per sample. Image analysis, base calling, and quality check was performed with the Illumina data analysis pipeline RTA3.4.4 and Bcl2fastq v2.20.

3.1.4 RNA sequencing analysis

RNA-seq reads were mapped to the human reference genome GRCh37 using Hisat2 (KIM; PAGGI; PARK; BENNETT *et al.*, 2019). Reads were counted into ensembl v75

genes with Htseq-count. One patient was excluded from further analysis due to a low number of aligned unique reads in both sorted populations (Table 2).

Table 2. Overview of the results obtained for HLA class II positive cHL cases used to sort CD4+ T cells for bulk RNA-seq

				Flow cytometry			%>=Q30		Total number of raw reads		Total number of reads aligned		Number of unique reads aligned	
Case	Histolygy	EBV	HLA-II	CD4+	CD4+CD26-	CD4+CD26+	CD4+CD26-	CD4+CD26+	CD4+CD26-	CD4+CD26+	CD4+CD26-	CD4+CD26+	CD4+CD26-	CD4+CD26+
cHL1	NS	Neg	Pos	48	78	22	90.1	89.9	60114052	53577190	59440241	52916065	51325667	44493053
cHL2	NS	Pos	Pos	16	74	26*	90.4	NA	75417874	NA	74007623	NA	40964672	NA
cHL3	NS	Pos	Pos	16	76	24	90.8	91.1	82591834	98128764	81570076	96276479	53467612	59908171
cHL4	NS	Neg	Pos	23	69	31	90.1	90.4	53877334	67208522	53171174	66376872	43174986	45573445
cHL5	LR	Pos	Pos	38	81	19	89.8	91.4	90873584	71404732	89541316	70642648	68596868	58490586
cHL6	LR	Neg	Pos	43	70	30	89.5	89.5	74471994	60434830	73429894	59612108	57962935	43839588
cHL7	NS	Neg	Pos	35	43	57	90.6	90.3	63839052	83284486	63021469	82416279	51117425	65629191
cHL8	NS	Pos	Pos	39	36	64	90.3	90.1	54983662	61844556	54368627	61074716	47295726	47977256
cHL9	NS	Neg	Pos	21	67	33*	89.8	NA	59956912	NA	59169847	NA	40884590	NA
cHL10	NOS	Pos	Pos	45	58	42	90.4	90.2	77451216	55415780	76589818	54723834	62644629	43935730
cHL11	NS	Pos	Pos	47	82	18	90.4	91.0	63283726	64524452	62604698	63808736	51205628	53235762
cHL12	NS	Neg	Pos	21	68	32	89.7	89.5	59023568	56166156	58362209	55369851	48843500	45680654
cHL13	NS	Pos	Pos	60	70	30	89.4	89.8	50705684	63912686	50091200	63027639	43209591	49517575
cHL14	NS	Neg	Pos	39	88	12	90.9	90.4	70762148	50928816	70001228	50246631	56763336	27561527
cHL15	MC	Neg	Pos	59	62	38	90.1	90.5	64925868	90989224	63990742	89814111	49729551	70758726
cHL16	MC	Neg	Pos	91	59	41	90.0	89.6	51859360	59883880	50873454	59222310	36411849	51079236
cHL17	NS	Neg	Pos	80	89	11	90.3	89.9	55957278	55399298	55337313	54722710	47204985	39689062
cHL18	NS	Neg	Pos	39	92	8*	91.0	NA	95744502	NA	94588428	NA	65998429	NA
cHL19**	NS	Neg	Pos	29	76	24	89.4	88.3	51645708	50626264	50004908	49386087	8693792	13862008

Analysis and visualization of RNA-seq data were performed in the R statistical environment (version 4.0.2). Normalization and differential expression analysis (DEA) was performed by R/Bioconductor package DESeq2 (LOVE; HUBER; ANDERS, 2014). Genes were considered differentially expressed when the adjusted p-value ≤0.05 and −1< log2foldchange>1. Genes of interest were selected based on the following criteria: (i) protein coding gene; (ii) described presence in T cells, according to RNA levels in the Schmiedel dataset (see: https://dice-database.org) (SCHMIEDEL; SINGH; MADRIGAL; VALDOVINO-GONZALEZ *et al.*, 2018), and function, as found in PubMed searches; (iii) availability of antibodies; and (iv) moderate-to-high expression levels. Gene set variation analysis (GSVA) was utilized to measure enrichment for specific CD4+ T cell subsets within each sorted population with the R/Bioconductor package GSVA.[26] CD4 subset-specific gene sets were retrieved from a previous study (SCHMIEDEL; SINGH; MADRIGAL; VALDOVINO-GONZALEZ *et al.*). DESeq2's median of ratios, Regularized log transformation (rlog) and Variance Stabilizing Transformed (vst) values were used for

data visualization, clustering and GSVA, respectively. Bulk RNA-seq BAM files are deposited in the European Nucleotide Archive (ENA) at EMBL-EBI under accession number PRJEB46009.

3.2 Results

3.2.1 Sorting and RNA-sequencing of CD4+ T cell subsets in cHL

CD4+ T cells of 19 HLA class II positive cHL cell suspensions were sorted based on membranous CD26 expression. The mean percentage of CD4+CD26- T cells was 70% (range 36–92%) (Table 2). In 14/19 cases, the percentage of CD4+CD26- T cells was at least 2-fold higher compared to the percentage of CD4+CD26+ T cells, showing that CD4+CD26- T cells were usually dominant in the cHL TME. RNA was isolated from the sorted CD4+CD26- and CD4+CD26+ T cells, which was used for RNA-seq. The total number of aligned RNA-seq reads ranged from 49 to 96 × 10^6 (mean: 65 × 10^6) (Table 2). The fraction of mapped reads marked as a duplicate ranged from 12.8– to 2.4% (mean: 25.7%). Both samples of one patient were excluded from further analysis due to a low number of aligned unique reads. The number of unique reads of the samples included in the subsequent analyses ranged from 28–71 × 10^6 (mean: 50 × 10^6). Subsequent analyses based on RNA-seq compared CD4+CD26- and CD4+CD26+ T cells using GSVA to identify similarities with specific CD4+ T cell subset lineages and DEA to identify distinct gene expression profiles.

3.2.2 CD4+CD26- T cells in cHL share characteristics with antigen experienced CD4+ T cell subsets

The GSVA scores for eight distinct CD4+ T cell subset gene signatures described by Schmiedel *et al*. were determined for each sorted T cell subset. CD4+CD26- T cells were mainly enriched for memory Treg and T follicular helper (Tfh) gene signatures in comparison with CD4+CD26+ T cells, and also showed some overlap with Th17 cells (Figure 1).

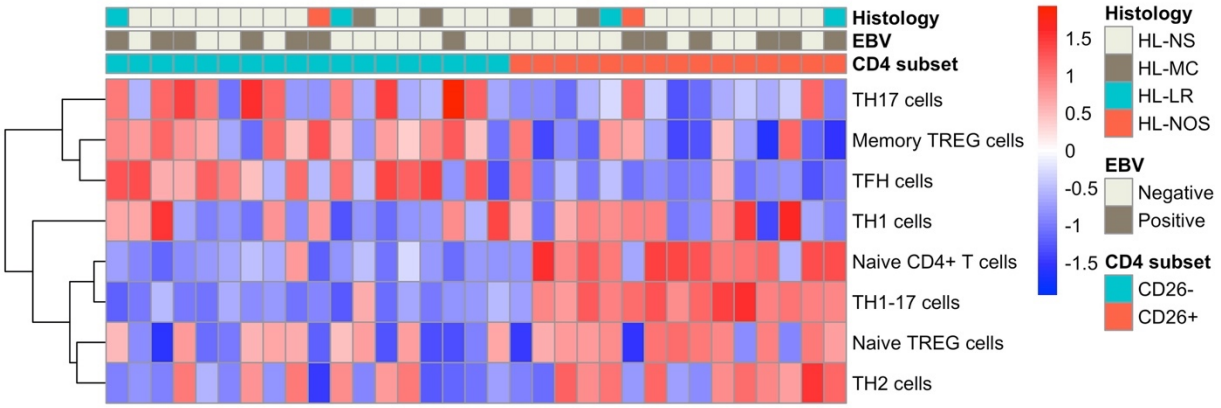

Figure 1. Supervised hierarchical clustering of GSVA-scores for CD4+ T cell subset gene signatures. Heatmap of the supervised hierarchical clustering of GSVA-scores for eight CD4+ T cell subset gene sets in 18 CD4+CD26- T cell populations and 15 CD4+CD26+ T cell populations. Supervised clustering is based on CD4 subset. NS = Nodular Sclerosis; MC = Mixed Cellularity; LR = Lymphocyte Rich; NOS = Not Otherwise Specified.

CD4+CD26+ T cells were mainly enriched for naïve CD4+ T cells and Th1/17 cells, and to a lesser extent for naïve Treg and Th2 cells, indicating that the CD4+CD26- T cells had a memory signature, while CD4+CD26+ T cells had a naïve signature. This indicated that CD4+CD26- T cells are more antigen experienced than CD4+CD26+ T cells.

3.2.3 The CD4+CD26- T cells have a distinct gene expression signature

Principal component analysis (PCA) considering the whole-gene expression profile revealed that samples separated based on CD26 expression status along PC1, the axis representing the highest variance in the data (Figure 2).

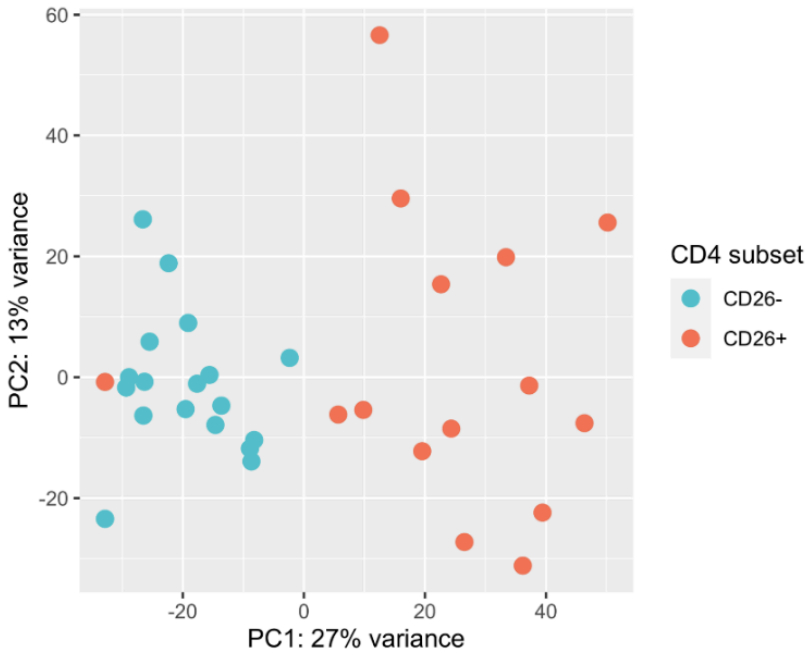

Figure 2. Principal Component Considering expression downstream data processing. First two components of the PCA. Dots represent individual samples, colors represent the different CD4+ T cell subsets.

This already suggested that CD4+CD26- and CD4+CD26+ T cells have distinct gene signatures. Comparison of the RNA-seq data of CD4+CD26- T cells to those of the CD4+CD26+ T cells resulted in identification of 567 differentially expressed genes (DEGs) (adjusted p-value <0.05 and −1< log2foldchange>1) (Figure 4). Of the 567 genes, 100 were upregulated and 467 downregulated in CD4+CD26- T cells.

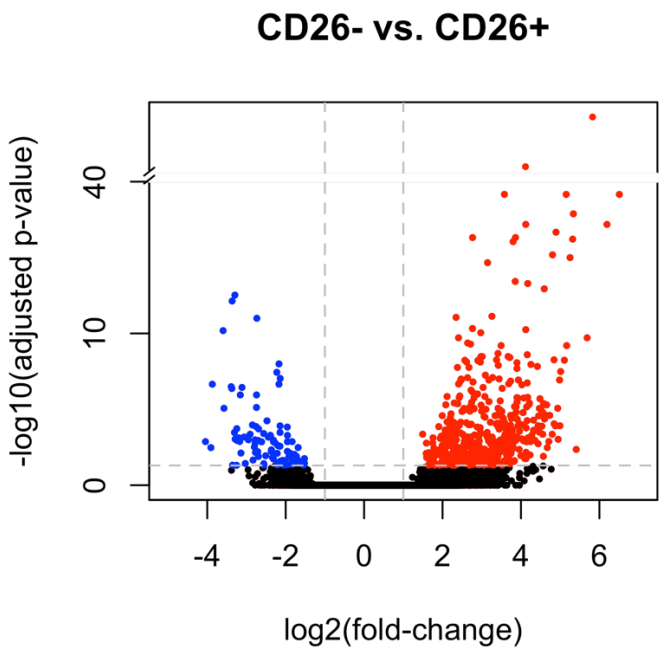

Figure 3. Volcano plot for CD4+CD26- versus CD4+CD26+ . – log10(adjusted p-values) are plotted against log2(foldchange). Red dots are indicating upregulated genes, blue dots are indicating dowregulated genes. Grey dashed lines indicate an adjusted p-value of <0.05 and a log2(foldchange) greater than 1 in both directions.

Of these, 100 genes were significantly upregulated and 467 genes were significantly downregulated in CD4+CD26- T cells compared to CD4+CD26+ T cells. Unsupervised hierarchical clustering of the 567 DEGs revealed two clusters with a clear separation between CD4+CD26- and CD4+CD26+ T cells (Figure 4). Within each T cell subset, no further clustering was observed for histological subtype or EBV status. The top DEG was DPP4 (CD26; log2foldchange = 5.83; padj = 5.45×10^{-45}) consistent with our sorting strategy.

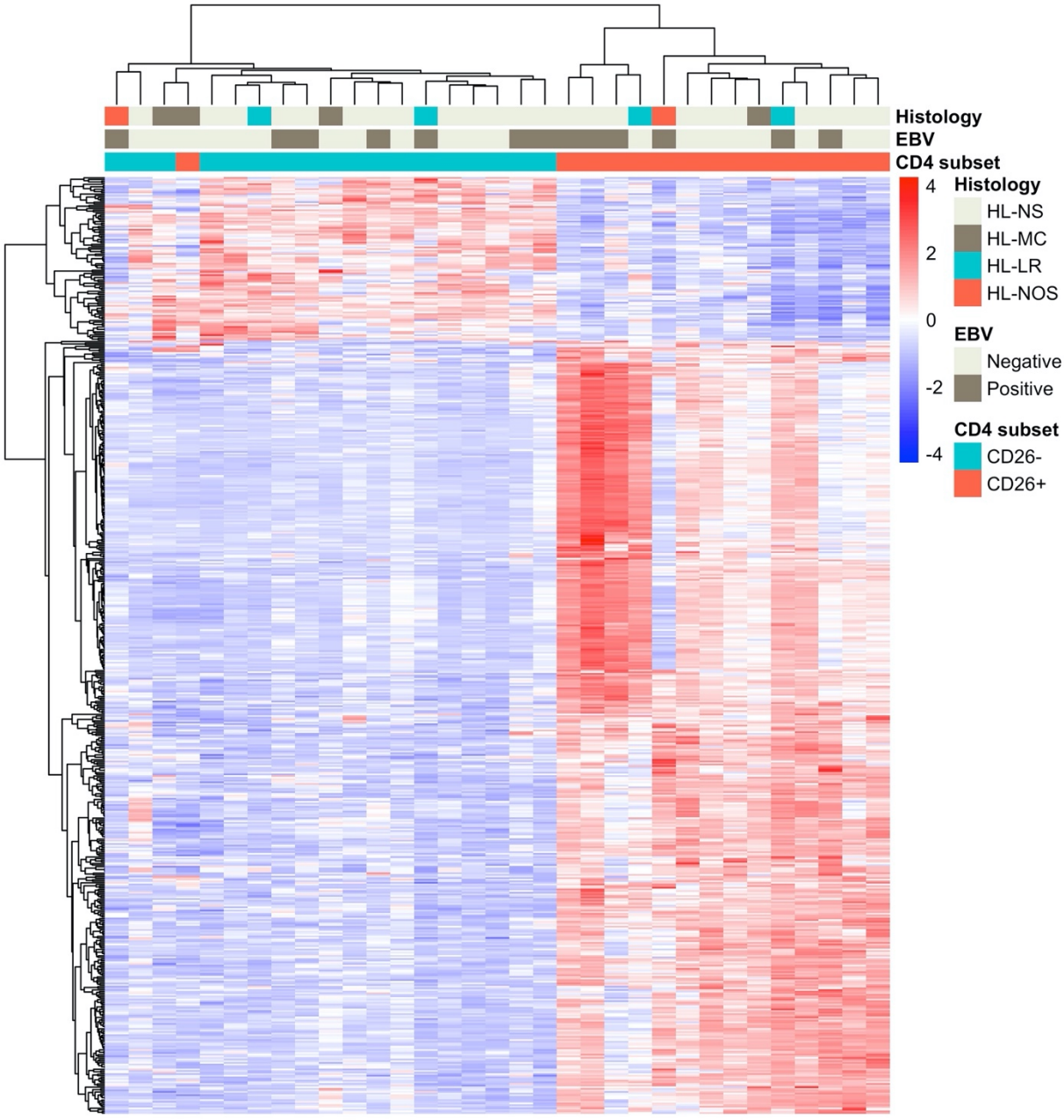

Figure 4. Heatmap showing the unsupervised hierarchical clustering of 567 genes differentially expressed between CD4+CD26- and CD4+CD26+ T cells. Rows are genes, columns are samples. NS = Nodular Sclerosis; MC = Mixed Cellularity; LR = Lymphocyte Rich; NOS = Not Otherwise Specified.

As we were interested in characterizing the CD4+CD26- T cells residing in proximity to the HRS cells we focused on the 100 genes significantly upregulated in this T cell population. Thus, CD4+CD26- T cells have increased expression of genes encoding for exhaustion associated transcription factors TOX and TOX2, transcription factor nuclear

factor I A (NFIA), immune checkpoints PD-1 and CD200, chemokine CXCL13 and actin-binding filament protein cortactin (CTTN).

3.3 Discussion

Using bulk RNA-seq approach, we have characterized the CD4+CD26- T cells in the cHL TME. Our results show that these CD4+CD26- T cells are antigen experience. Markers that were most prominently enriched in CD4+CD26- compared to CD4+CD26+ T cells and were expressed in the majority of rosetting CD4+ T cells were thymocyte selection-associated high-mobility group box (TOX) and TOX2, which are exhaustion associated transcription factors.

The finding that CD4+CD26- T cells in the TME of cHL displays an antigen experienced gene expression profile fits well with cHL associated T cell types that have been described in multiple previous reports (AOKI; CHONG; TAKATA; MILNE *et al.*, 2020; CADER; SCHACKMANN; HU; WIENAND *et al.*, 2018; FERRARINI; RIGO; ZAMÒ; VINANTE, 2019; MA; VISSER; BLOKZIJL; HARMS *et al.*, 2008). Our group has recently established that initial interaction between T cells and HRS cells is fast and involved a large proportion of T cells (VELDMAN; VISSER; HUBERTS-KREGEL; MULLER *et al.*, 2020), which is consistent with antigen experienced T cells recognizing a broad spectrum of HRS cell derived antigens. These interactions occur by means of the immunological synapse, resulting in formation of T cell rosettes and low-level IL-2 production, suggesting that these T cells get activated, but only to some extent (VELDMAN; VISSER; HUBERTS-KREGEL; MULLER *et al.*, 2020). This low-level activation state is consistent with expression of early activation markers CD38 and CD69, while CD25 and CD26 are missing (MA; VISSER; BLOKZIJL; HARMS *et al.*, 2008; POPPEMA, 1996; TANAKA; CAMERINI; SEED; TORIMOTO *et al.*, 1992).

Our gene expression data suggest that these antigen experienced T cells consist of memory Treg cells and/or Tfh cells. However, further evidence for a contribution of Tfh cells in the cHL TME is lacking in literature and characteristic markers like BCL-6 and CXCR5 (ROIDER; SEUFERT; UVAROVSKII; FRAUHAMMER *et al.*, 2020) are not present in our differentially expressed gene set. Memory Treg cells have commonly been described and are actively recruited by HRS cells that attract them by secreting high

amounts of chemokines CCL17/TARC and CCL22/MDC (IELLEM; MARIANI; LANG; RECALDE *et al.*, 2001; ISHIDA; ISHII; INAGAKI; YANO *et al.*, 2006; NIENS; VISSER; NOLTE; VAN DER STEEGE *et al.*, 2008). Thus, memory Treg constitute a major source of CD4+ T cells in the cHL TME.

Besides the already known characteristic feature of being CD26-, we identified two additional proteins enriched in CD4+ T cells in the TME. These proteins, i.e. TOX and TOX2, were also frequently expressed by rosetting T cells in cHL. The TOX protein family consists of four members that all function as transcription factors: TOX (also known as TOX1), TOX2, TOX3 and TOX4 (LIANG; HUANG; ZHAO; CHEN *et al.*, 2021). TOX and/or TOX2 are involved in many early lymphoid developmental processes, including positive selection in thymocytes, early development of CD4+ T and NK cells, development of innate lymphoid cells and lymph node organogenesis (ALIAHMAD; KAYE, 2008; VONG; LEUNG; HOUSTON; LI *et al.*, 2014; YU; LI, 2015). Corresponding with our DEG, TOX can induce the expression of the Tfh defining chemokine CXCL13, and immune checkpoint molecule PD-1, which is a well-established marker of exhaustion (WANG; HE; SHEN; XIA *et al.*, 2019; XU; ZHAO; WANG; FENG *et al.*, 2019; YAO; SUN; LACEY; JI *et al.*, 2019)42. Induction of exhaustion by TOX and TOX2 is the inability of CD4+ CD26- T cells to upregulate production of several cytokines upon *in vitro* stimulation (MA; VISSER; BLOKZIJL; HARMS *et al.*, 2008). It is well known that TOX and TOX2 are both induced by chronic antigen stimulation of the TCR (ALFEI; KANEV; HOFMANN; WU *et al.*, 2019; SCOTT; DÜNDAR; ZUMBO; CHANDRAN *et al.*, 2019; SEO; CHEN; GONZÁLEZ-AVALOS; SAMANIEGO-CASTRUITA *et al.* ; YAO; SUN; LACEY; JI *et al.*, 2019). It would be interesting to study if this is also the case in HL, given the importance of HLA class II-TCR interactions in HL rosetting (VELDMAN; VISSER; HUBERTS-KREGEL; MULLER *et al.*, 2020).

Increased TOX levels in T cells are very prominent in our study in cHL and have also been described in solid malignancies and B cell non-Hodgkin lymphoma (HUANG; LIANG; ZHAO; DENG *et al.*, 2022; KIM; PARK; PARK; KIM *et al.*, 2020; MAESTRE; GARCÍA-GARCÍA; JIMÉNEZ; REYES-GARCÍA *et al.*, 2020; WANG; HE; SHEN; XIA *et al.*, 2019). Interestingly, several lines of evidence support a role of TOX and TOX2 in CD8+ T cells in sensitivity to immune checkpoint blockade. Knockdown of TOX in CD8+ T

cells in a patient-derived xenograft mouse model of hepatocellular cancer decreased tumor growth, alleviated the CD8+ T cell exhaustion, increased CD8+ T cell infiltration and improved responses to PD-1 blockade therapy (WANG; HE; SHEN; XIA *et al.*, 2019). In addition, CD8+ chimeric antigen receptor (CAR) T cells with a combined deficiency in TOX and TOX2 were more active and promoted profound tumor regression and prolonged survival in a melanoma mouse model (SEO; CHEN; GONZÁLEZ-AVALOS; SAMANIEGO-CASTRUITA *et al.*). If these results in CD8+ T cells can be extrapolated to CD4+ T cells in cHL several important implications arise. First, cHL has a very high response rate to PD-1 blockade with objective response rates as high as 87% in the relapsed and refractory setting with also excellent efficacy in first-line treatment combined with concomitant or sequential de-intensified chemotherapy regimens in ongoing trials (BRÖCKELMANN; GOERGEN; KELLER; MEISSNER *et al.*, 2020; MERRYMAN; ARMAND; WRIGHT; RODIG, 2017; RAMCHANDREN; DOMINGO-DOMÈNECH; RUEDA; TRNĚNÝ *et al.*, 2019; VOLTIN; METTLER; VAN HEEK; GOERGEN *et al.*, 2021). Reversal of exhaustion in CD4+ T cells is likely responsible for these very high response rates because of their high abundance, their importance to survival of HRS cells and their predictive role in response to PD-1 blockade (CADER; HU; GOH; WIENAND *et al.*, 2020; LIU; SATTARZADEH; DIEPSTRA; VISSER *et al.*, 2014; ROEMER; REDD; CADER; PAK *et al.*, 2018; VELDMAN; VISSER; HUBERTS-KREGEL; MULLER *et al.*, 2020). Second, the extent of exhaustion in CD4+ T cells is expected to be predictive for immune checkpoint blockade outcome and it would be interesting to study TOX and TOX2 expression in this setting. Finally, targeting TOX and/or TOX2 with small molecule inhibitors (AGRAWAL; SU; HUANG; HSING *et al.*, 2019), might revert T cell exhaustion, thereby being an attractive way to further improve immunotherapy results in cHL.

4 VERIFY THE REPRODUCIBILITY OF PUBLISHED GENE EXPRESSION SIGNATURES FOR DLBCL.

This specific aim was to reproduce four biology driven gene expression signatures in a large cohort of clinically well annotated DLBCL NOS/HGBCL samples from the HOVON-84 trial using the NanoString platform, which permits robust amplification free GEP analysis of RNA from formalin-fixed paraffin-embedded tissue with minimal background signal (VELDMAN-JONES; BRANT; ROONEY; GEH *et al.*). Selection of the four gene expression signatures was based on the biological features presenting COO, MYC activity, oxidative phosphorylation (OxPhos), B-cell receptor (BCR) signaling, and the TME as well as the potential reproducibility of the classifiers (FFPE based, number of genes, and availability of algorithms) (CAREY; GUSENLEITNER; CHAPUY; KOVACH *et al.*, 2015; KEANE; VARI; HERTZBERG; CAO *et al.*, 2015; MONTI; SAVAGE; KUTOK; FEUERHAKE *et al.*, 2005; SCOTT; WRIGHT; WILLIAMS; LIH *et al.*, 2014). In addition, we studied whether the reproducible gene expression profiles are independent of each other and whether their combined use can indicate distinct DLBCL NOS/HGBCL subgroups. Finally, we tested potential associations with clinical features in a well-defined population of patients with DLBCL NOS/HGBCL.

4.1 Materials and Methods

4.1.1 Patient Cohort

HOVON-84 is a multicentric, randomized phase III trial, with no benefit of the intensification of rituximab combined with 2-weekly CHOP chemotherapy in patients with newly diagnosed DLBCL. At the time of the study HGBCL DH was not considered a distinct entity and as such was included in the trial (LUGTENBURG; BROWN; HOLT; D'AMORE *et al.*, 2020). The study was conducted in accordance with the ethical guidelines mandated by the Declaration of Helsinki and approved by all relevant institutional review boards or ethical committees. Written informed consent, including use of biopsy material for research purposes, was obtained from all patients. The HOVON-84 trial included 574 patients and good quality NanoString (Seattle, WA, USA) data could be generated for 175 patients. This cohort forms the core of the present study. In the other

399/574 patients, no representative formalin-fixed paraffin embedded (FFPE) biopsy material was available for this study (blocks not available for study, blocks exhausted, or insufficient quality) or NanoString data were of insufficient quality. Clinical characteristics of the 175 HOVON-84 patients studied in this report as well as the characteristics of the total cohort and the original GEP signatures cohorts are listed in Table 3.

Table 3. Overview of characteristics of the HOVON-84 and previously published cohorts.

Characteristic	**HOVON-84 (all patients)**	**HOVON-84 (current study)**	**Scott et al 2014**	**Monti et al 2005**	**Carey et al 2015**	**Keane et al 2015**
Patients n	574	175	119	176	70	158
Prospective	Yes	Yes	No	Yes	No	Yes
Number of centers	>10	>10	10	1	2	4
Females n (%)	275 (48)	89 (51)	48 (40)	84 (48)	32 (47) – 2 NA	66 (42)
Age≥60 years n (%)	396 (69)	116 (66)		112 (64)	38 (56) – 2 NA	..
Stage II n (%)	114 (20)	40 (23)	53 (46)	53 (32)	..	..
Stage III/IV n (%)	460 (80)	135 (77)	63 (54) – 3 NA	115 (68) – 8 NA	..	..
Extranodal sites >1 n (%)	..	..	13 (12) – 11 NA	21 (12) – 2 NA	..	..
LDH elevated n (%)	379 (66)	104 (59)	53 (55) – 22 NA	81 (56) – 31 NA	..	..
IPI good risk n (%)	246 (43)[aa]	84 (48)[aa]	71 (66)	82 (57)	..	..
IPI poor risk n (%)	328 (57)[aa]	91 (52)[aa]	37 (34) – 11 NA	62 (43) – 32 NA	..	64 (42) – 6 NA
Treatment	R-CHOP	R-CHOP	..	CHOP-based	R-CHOP	R-CHOP
OS events n (%)	164 (29)	37 (21)	..	76 (43)	..	36 (23)
COO ABC n (%)	151 (38)[a]	61 (34)*	49 (41)*	24 (18)[b]	26 (39)[a]	54 (34)[b]

COO GCB n (%)	242 (62)[a] – 181 NA	95 (53)*	48 (40)*	106 (82)[b] – 46 NA	40 (61)[a] – 4 NA	104 (66)[b]

Percentages were calculated under available data. The number of samples with unavailable data are described with NA. aa Age adjusted IPI. * COO based on Lymph2Cx algorithm; a COO based on Hans algorithm; b COO based on Bayesian classifier of 19 genes as previously described by Wright et al.; The treatment is randomized between R-CHOP and RR-CHOP for HOVON-84 cohort with no significant difference between the two groups. NA, not available.

No statistically significant differences were observed between the cases included in the present study and the entire HOVON-84 cohort, making the samples used in this study a representation of the entire cohort. (Gender p-value = 0.5; Age p-value = 0.5; Stage p-value = 0.3; LDH levels p-value = 0.1; aaIPI p-value = 0.2; OS p-value = 0.06; COO p-value = 0.9.)

4.1.2 Immunohistochemistry

Immunohistochemistry (IHC) was performed as part of previous studies by the Lunenburg Lymphoma Biomarker Consortium (North Bethesda, MD, USA) (ROSENWALD; BENS; ADVANI; BARRANS *et al.*, 2019; SALLES; DE JONG; XIE; ROSENWALD *et al.*, 2011) and available for 167 DLBCL patients for CD10, MUM1, and BCL6. In addition, BCL2 and MYC IHC was performed for 161 DLBCL patients using routine diagnostic procedures on tissue microarrays. Scoring of CD10, MUM1, and BCL6 staining and subsequent classification as GCB or non-GCB was performed according to the Hans algorithm (HANS; WEISENBURGER; GREINER; GASCOYNE *et al.*, 2004). MYC IHC was scored as the percentage of positive tumor cells as estimated by an experienced hematopathologist in 10% increments. Lymphomas were defined as double expressors (DE) based on MYC positivity in ≥40% and BCL2 positivity in ≥50% of the tumor cells (HU; XU-MONETTE; TZANKOV; GREEN *et al.*, 2013). For correlation to the MYC gene signature as published by Carey et al., we used a cutoff of ≥50% positive tumor cells for MYC-High and <50% for MYC-Low consistent with the cutoff as defined in this paper. For MHC-II (HLA-II), IHC was performed on tissue microarrays and cores were

scored for intensity of staining. No or weak staining was classified as MHC-II low and all other cases were classified as MHC-II high (NIJLAND; VEENSTRA; VISSER; XU *et al.*).

4.1.3 Detection of Chromosomal Translocations in BCL2, BCL6, and MYC

Fluorescence in situ hybridization (FISH) for MYC, BCL2, and BCL6 was performed on 152, 148, and 153 cases, respectively, with break apart probes from Vysis LSI, Abbott (Chicago, IL, USA). Scoring was performed as described previously (ROSENWALD; BENS; ADVANI; BARRANS *et al.*, 2019; SALLES; DE JONG; XIE; ROSENWALD *et al.*, 2011). In addition to the FISH, targeted NGS was performed for 140 samples to identify structural variants (SV) in MYC, BCL2, and BCL6 using the protocols as previously described (MENDEVILLE; ROEMER; VAN DEN HOUT; LOS-DE VRIES *et al.*, 2019). The SV information was combined with the FISH results to classify cases as HGBCL DH, regarding all cases with a positive result for either FISH (8) or NGS (7) or both (125) as positive.

4.1.4 Gene Expression Profiling

For a total of 175 samples, we were able to obtain sufficient good quality RNA with FFPE RNeasy Kit (Qiagen, Hilden, Germany) for analysis on the NanoString Platform. The core set of probes for 117 genes (Table 4) was hybridized to 100–200 ng of RNA for 16 h at 65 ◦C. Samples were loaded on an nCounter SPRINT Cartridge and processed on the nCounter SPRINT™ Profiler. The expression data were analyzed using Nanostring's nSolver analysis software (version 3.0). Registered counts passing the standard QC parameters were used for further analysis. The normalized data were scaled and transformed to log2.

Table 4. List of genes used to classify the four GEP using quantification by the Nanostring platform.

GeneID	Signature	GeneID	Signature	GeneID	Signature
TNFRSF13B	COO	**PRMT1**	MYC activity	**DDX11**	Consensus clustering
LIMD1	COO	**LDHB**	MYC activity	**UBA1**	Consensus clustering
IRF4	COO	**TRAP1**	MYC activity	**PLCG2**	Consensus clustering

CREB3L2	COO	**AHCY**	MYC activity	**CD22**	Consensus clustering
PIM2	COO	**LRP8**	MYC activity	**SIPA1L3**	Consensus clustering
CYB5R2	COO	**EBNA1BP2**	MYC activity	**CD79A**	Consensus clustering
RAB29	COO	**CDK4**	MYC activity	**CD37**	Consensus clustering
CCDC50	COO	**ETFA**	MYC activity	**PMS2P9**	Consensus clustering
R3HDM1	COO	**UCK2**	MYC activity	**PAX5**	Consensus clustering
WDR55	COO	**CTPS1**	MYC activity	**PMS2P2**	Consensus clustering
ISY1	COO	**GOT2**	MYC activity	**EZR**	Consensus clustering
UBXN4	COO	**TMEM97**	MYC activity	**MAP4K1**	Consensus clustering
TRIM56	COO	**RRS1**	MYC activity	**INPP5D**	Consensus clustering
MME	COO	**DDX21**	MYC activity	**LAMP1**	Consensus clustering
SERPINA9	COO	**PHB2**	MYC activity	**TNFRSF1A**	Consensus clustering
ASB13	COO	**WDR3**	MYC activity	**SELPLG**	Consensus clustering
MAML3	COO	**KIAA0101**	MYC activity	**CTSB**	Consensus clustering
ITPKB	COO	**FASN**	MYC activity	**IFITM1**	Consensus clustering
MYBL1	COO	**SAMD13**	MYC activity	**GATA3**	Consensus clustering
S1PR2	COO	**CDC25A**	MYC activity	**MAF**	Consensus clustering
MYC	MYC activity	**LYAR**	MYC activity	**SLAMF8**	Consensus clustering
SRM	MYC activity	**SLC12A8**	MYC activity	**SERPING1**	Consensus clustering
AKAP1	MYC activity	**P2RY12**	MYC activity	**TCIRG1**	Consensus clustering
NME1	MYC activity	**TMEM119**	MYC activity	**IL6R**	Consensus clustering
FBL	MYC activity	**SHISA8**	MYC activity	**CD2**	Consensus clustering
RFC3	MYC activity	**SLAMF1**	MYC activity	**TNFSF13**	Consensus clustering
TCL1A	MYC activity	**COX7A2L**	Consensus clustering	**CD3E**	Consensus clustering
POLD2	MYC activity	**PSMA6**	Consensus clustering	**DAB2**	Consensus clustering
RANBP1	MYC activity	**RPLP0**	Consensus clustering	**CD6**	Consensus clustering
GEMIN4	MYC activity	**MRPL3**	Consensus clustering	**IRF1**	Consensus clustering
MRPS34	MYC activity	**NDUFB1**	Consensus clustering	**MAFB**	Consensus clustering
DHX33	MYC activity	**ATRAID**	Consensus clustering	**ITGB2**	Consensus clustering
PPRC1	MYC activity	**PSMA5**	Consensus clustering	**CXCL12**	Consensus clustering
PPAT	MYC activity	**PSMA2**	Consensus clustering	**GRN**	Consensus clustering
FAM216A	MYC activity	**SOD1**	Consensus clustering	**CD4**	Immune ratio
PAICS	MYC activity	**MRPL15**	Consensus clustering	**CD8**	Immune ratio
UCHL3	MYC activity	**DBI**	Consensus clustering	**CD163**	Immune ratio
NOLC1	MYC activity	**XRCC5**	Consensus clustering	**CD68**	Immune ratio
RUBCNL	MYC activity	**MKI67**	Consensus clustering	**PDL1**	Immune ratio

4.1.5 COO Classifier

For COO classification, raw counts obtained by NanoString gene expression analysis for all genes of the algorithm were uploaded at the Lymphoma/Leukemia Molecular Profiling Project (LLMPP) website (https://llmpp.nih.gov/LSO/LYMPHCX/lymphcx_predict.cgi, accessed on 12 September 2017) to run the Lymph2Cx classifier (SCOTT; WRIGHT; WILLIAMS; LIH *et al.*, 2014).

4.1.6 MYC Activity Score

To reproduce the MYC activity score we used the selection and bioinformatics strategy as reported by Carey et al., since the algorithm is not publicly available. In brief, we used their original training cohort as training set of the elastic net classifier. This training set included 14 cases scored as MYC-low based on positive staining in <40% of the tumor cells and 16 cases as MYC-high based on positive staining in >60% of the tumor cells. The classifier was subsequently applied to the HOVON-84 (n = 175) test set. The training dataset was normalized with the R package NanoStringNorm (WAGGOTT; CHU K FAU - YIN; YIN S FAU - WOUTERS; WOUTERS BG FAU - LIU *et al.*), considering the sum of the expression values to estimate the technical assay variation, the mean to estimate background count levels, and the sum of the six housekeeping genes to normalize for the RNA sample content. In addition, the data were log2 transformed. The alfa and gamma parameters were set at 0.1 and the classification accuracy was assessed with the Leave One Out Cross Validation (LOOCV), as in the original publication. A cutoff of 0.5 was used to stratify the tumors with high and low MYC activity score. The importance of each gene was calculated based on combinations of the absolute values of the weights as reported by (GEVREY; DIMOPOULOS; LEK, 2003). All the analyses were conducted with the R package caret (KUHN, 2008). The spearman's correlation was used to evaluate the association between the MYC activity score and MYC IHC values and the predictions were compared with the outcome of the IHC staining.

4.1.7 Monti Consensus Clustering

Briefly, the three consensus clustering approaches applied were Hierarchical Clustering (HC) considering the Euclidean distance, Self-Organizing Maps (SOM) with the R packages ConsensusClusterPlus (WILKERSON; HAYES) and Kohonen (WEHRENS; KRUISSELBRINK, 2018), and the Gaussian Finite Mixture Models algorithm (which represents the probabilistic clustering (PC)) using the R package mclust (SCRUCCA; FOP; MURPHY; RAFTERY). To define the best number of clusters, we used 80% of resampling on 200 replicates for each clustering algorithm, as in the original paper. Consensus matrices including two to nine clusters were built and evaluated by the relative change in area under CDF curves or Bayesian Information Criterion (BIC) metrics. Confusion matrices were used to determine the number of samples assigned to similar clusters by any 2 algorithms. HOVON-84 samples with the same classification by all three algorithms (“metaconsensus”) were defined as samples belonging to the main clusters. For the remaining HOVON-84 samples, we built a naive-Bayes classifier with the R package caret (KUHN, 2008). The naïve-Bayes classifier was first trained with the samples from the original meta-consensus clustering study and subsequently used to predict the cluster membership for the remaining HOVON-84 samples, similar to the approach applied in the original publication.

4.1.8 Immune Ratio

To reproduce the prognostic marker based on the expression ratio between immune effectors and inhibitory (immune checkpoint) genes, we followed the approach as published by Keane et al.. We decided to focus on their main finding, which was the prognostic significance of the CD4 × CD8 to CD163:CD68 × PD-L1 ratio. This immune ratio was additive and independent to the revised-IPI and COO in the original paper. The ratio was calculated using the log2 scaled gene expression values and to assess the prognostic value of this ratio in the HOVON-84 cohort we used the Keane proposed cut-off (−0.278958829) to stratify samples into high and low expression ratio subgroups.

4.1.9 Statistical Analysis

To compare categorical data, we used Fisher's Exact Test or the X2 test, where applicable. The Kaplan–Meier method was used to estimate the overall survival (OS) and progression free survival (PFS). Univariable and multivariable Cox proportional hazard regression models and Wald p-values were used to evaluate the prognostic impact and statistical significance. All the analyses were performed in R 3·6·2 (TEAM, 2019). We did not separately analyze patients per study treatment arm since PFS and OS were similar, and treatment regimens differed on Rituximab-dose only. Patients with significant therapy protocol violations were not included.

4.2 Results

4.2.1 Study Design

In addition to the widely used COO signature to classify DLBCL cases (Scott et al. 2014), we prioritized three additional signatures that were NanoString based, since it is a reproducible technology by different laboratories, available at that time, and reflected different biological aspects. The three selected signatures included MYC activity score (Carey et al. 2015), Monti consensus clustering (Monti et al. 2005), and the immuneratio signature (Keane et al. 2015). As the COO classifier and immune ratio classifiers were both based on a limited number of genes, we included all genes and applied the published algorithms. For the two much larger classifiers, i.e., MYC activity score and the consensus clustering, with algorithms that had to be re-designed, we followed a different approach. We first recreated the clustering and/or classification algorithms and tested their performance on the originally reported cohorts, with the original set of genes. To make a subsequent clinical application feasible, we reduced the gene list, by prioritizing the genes with the strongest contributions to the algorithms and applied the validated algorithms on the original cohorts to establish the effectivity of our selected gene set.

4.2.2 Performance of the MYC Activity Score Using a Subset of the Genes

The MYC activity score algorithm was first reproduced in the Carey cohort using the original set of 61 genes (Figure 5A). Next, we tested the validated algorithm on our subset consisting of 34 genes (Figure 51B).

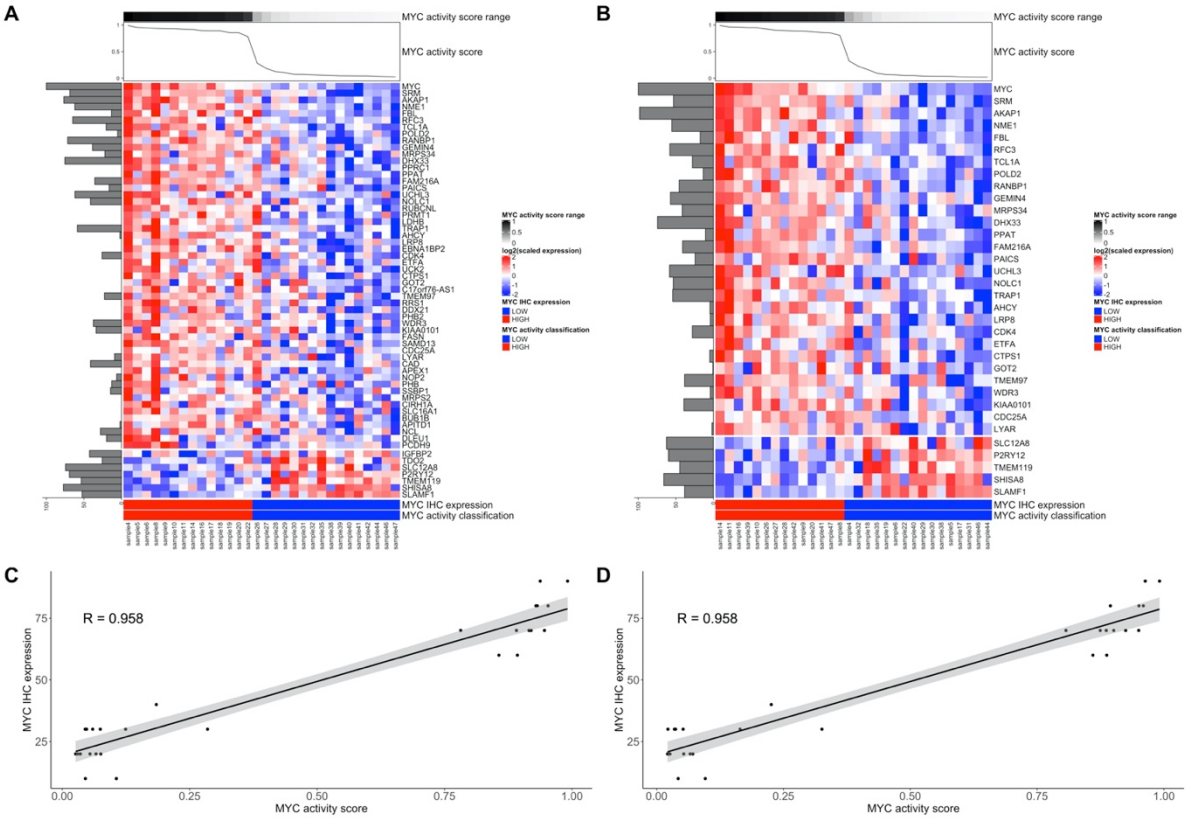

Figure 5. MYC activity classifier for the original Carey training cohort. (a) Heatmap with relative expression levels of the 61 genes including the relative contribution of each gene to the classifier (horizontal, shaded bar graph) and the MYC activity score (line graph). (b) Heatmap with relative expression levels of the 27 genes selected for our study including the relative contribution of each gene to the classifier (horizontal, shaded bar graph) and the MYC activity score (line graph). (c) Spearman's correlation between MYC activity score and MYC IHC expression for the 30 samples of the Carey training cohort considering 61 genes in the model. (d) Spearman's correlation between MYC activity score and MYC IHC expression for the 30 samples of the Carey training cohort considering 45 genes in the model. The selected set of 45 genes recapitulates the original MYC activity clusters.

Although the impact of the genes in the classifier was different from the original publication for both gene sets (CAREY; GUSENLEITNER; CHAPUY; KOVACH *et al.*, 2015), MYC had the highest impact consistent with the original paper. We observed a

good correlation between the MYC activity score and the percentage of tumor cells staining positive for MYC in the Carey training set cases using both the initial gene set and the subset included in our analysis (Figure 5C,D). Moreover, we observed a perfect match of the MYC activity score with the MYC expression as determined by IHC in the training set (Table 5).

Table 5. Performance of MYC activity classifier in the Carey training and HOVON-84 test sets.

Metric	Carey training dataset (30 samples)	HOVON-84 dataset (161 samples)
Accuracy	1	0.65
Sensitivity*	1	0.65
Specificity	1	0.65
PPV	1 (30/30)	0.43 (105/161)
NPV	1 (0/30)	0.82 (56/161)
Spearman's correlation	0.96	0.48

Only cases with matched MYC IHC and MYC activity scores were included. The total number of samples equally and not equally classified in comparison to MYC IHC expression are in parenthesis. *The sensitivity refers to the ability of the test to identify tumors with high MYC IHC expression (>50%) as having MYC activity score >0.5.

4.2.3 Performance of the Monti Consensus Clustering Algorithm Using a Subset of the Genes

We first reproduced the Monti consensus clustering into Oxidative phosphorylation (OxPhos), B-cell Receptor/Proliferation (BCR), and Host response (HR) groups using the dataset of Monti et al.. The three algorithms revealed three subgroups consistent with the original Monti publication using 1112 annotated genes from the 2118 microarray probes. Meta-consensus clustering revealed an initial classification of 115 out of 176 samples (Figure 6A).

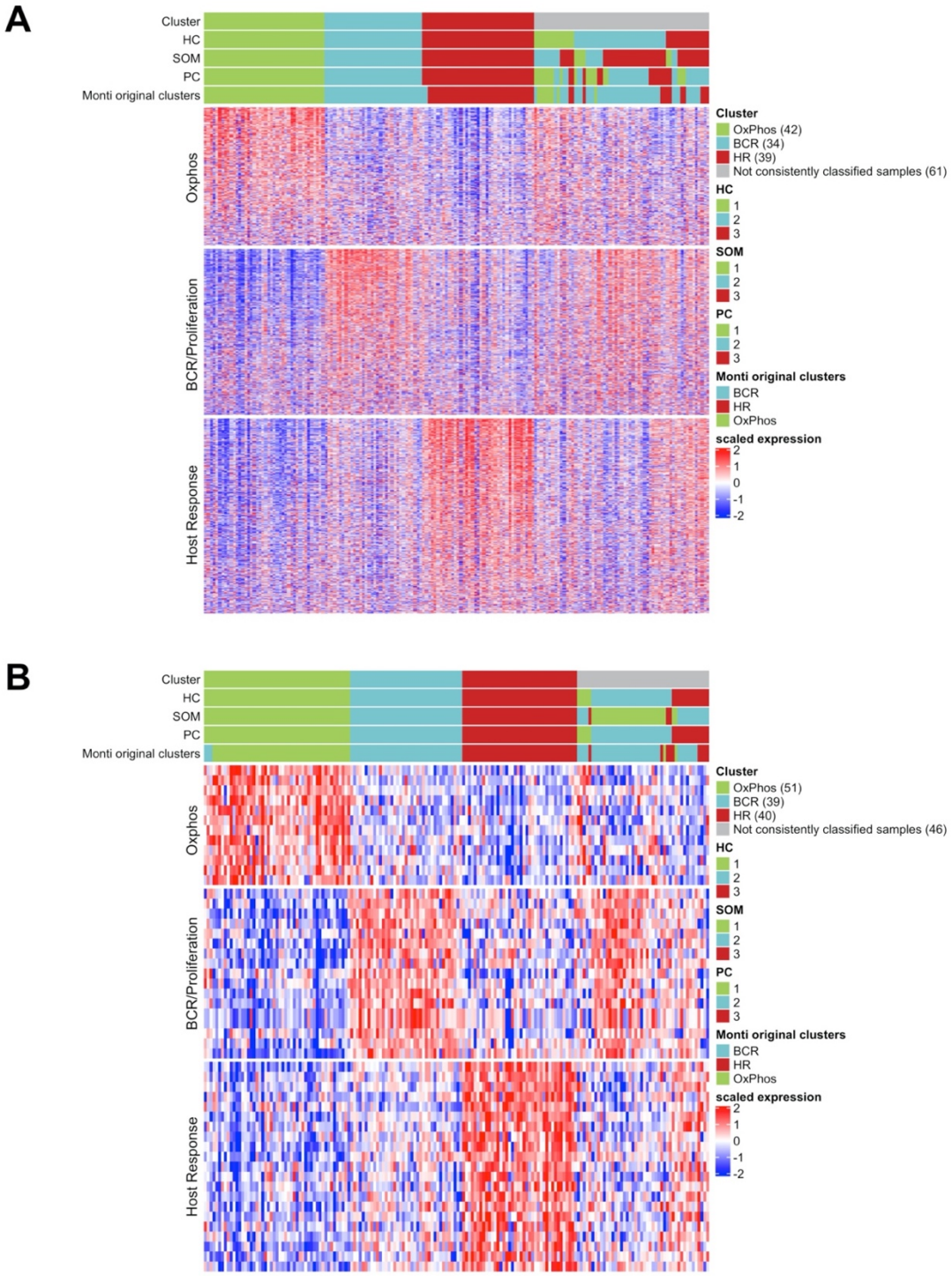

Figure 6. Consensus clusters in original Monti cohort. (**a**) Heatmap indicating the three identified clusters applying our algorithm using all 2118 Monti probes. The upper bars represent the classification of the meta-consensus clusters, hierarchical clustering (HC) only, self-organized maps (SOM) only, probabilistic clustering (PC) only and the original Monti defined clusters, respectively. Two samples were misclassified comparing the meta-consensus clusters to the original Monti classes (**b**) Heatmap indicating the three identified clusters applying our algorithm using the 50 selected probes.

The upper bars represent the samples classification of the meta-consensus clusters, hierarchical clustering (HC) only, self-organized maps (SOM) only, probabilistic clustering (PC) only and the original Monti defined clusters, respectively. Three samples were misclassified comparing the meta-consensus clusters to the original Monti classes.

This showed that our algorithm correctly recapitulates the original clustering patterns as reported by Monti et al.. After successful reproduction of the original clustering pattern, we evaluated the performance of the algorithm on our selected subset of genes, which included probes ranking in the top 50 most relevant probes to define each of the three biologic clusters, as specified by Monti. In total, this gene set comprised 47 out of 1112 annotated genes (12 out of 342 OxPhos related genes, 14 out of 344 BCR/Proliferation related genes, and 21 out of 427 HR related genes). This revealed for 130 of the 176 samples of the Monti cohort a consistent clustering, indicating that our selection of genes correctly assigned the majority of the samples to the three clusters (Figure 6B).

4.2.4 COO Classifier in HOVON-84

Application of the COO classifier revealed 94 (54%) GCB, 58 (33%) ABC, and 23 (13%) unclassified cases (Figure 7).

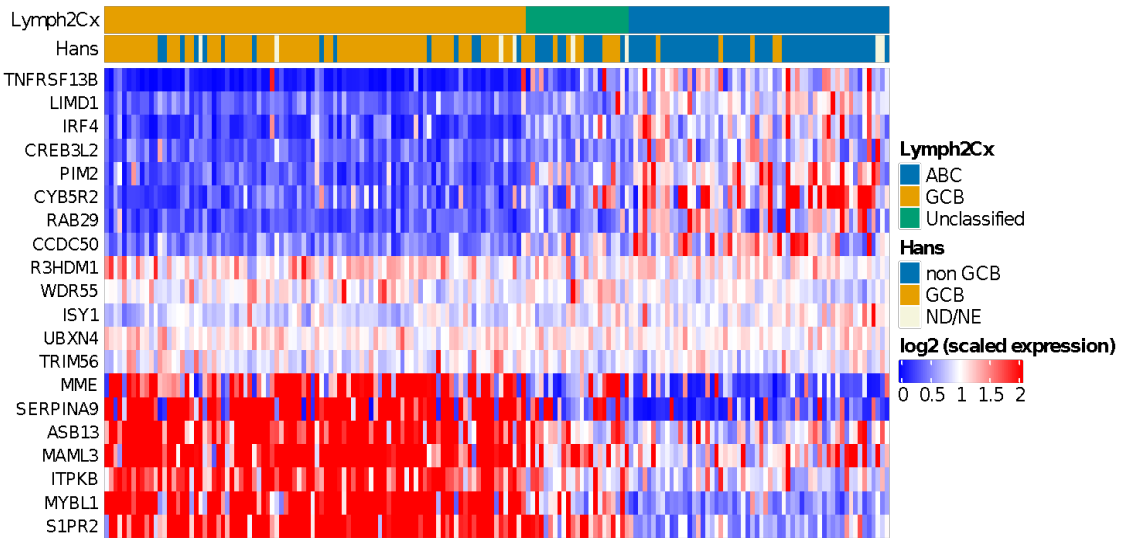

Figure 7. Heatmap showing relative expression levels of the COO genes used to classify cases using the Lymph2Cx algorithm. A clearly distinct gene expression pattern can be observed for ABC and GCB subtype DLBCL cases.

According to Hans classification, 91 cases (54%) were classified as GCB and 76 (46%) as non-GCB. We observed a significant association ($p < 0.00001$) between the COO classifier and the Hans algorithm (Table 6).

Table 6. Comparison of cell of origin (COO) allocation between COO classifier and Hans' algorithm.

						Hans's algorithm		
Lymph2Cx (GEP)	**N**	**IHC Sensitivity**	**IHC Specificity**	**IHC PPV**	**IHC NPV**	**Non-GCB (n=76)**	**GCB (n=91)**	**Not scored (n=8)**
ABC (33%)	58	91%	84%	78%	94%	51	5	2
GCB (54%)	94	84%	84%	94%	78%	14	76	4
Unclassified (13%)	23	..	..	..	..	11	10	2

Unclassified and not scored cases were excluded from calculations. ABC, activated B-cell; GCB, germinal center B-cell; GEP, gene expression profiling; IHC, immunohistochemistry; NPV, negative predictive value; PPV, positive predictive value.

Sensitivity and specificity values were 91% and 84% for ABC and non-GCB comparison and 84% and 91% for GCB classes, as previous reported (YOON; AHN; YONG YOO; JIN KIM *et al.*, 2017). We also found that ABC cases were enriched in older patients (>60 years) ($p < 0.002$), as reported by Klapper et al. in 2012 (KLAPPER; KREUZ M FAU - KOHLER; KOHLER CW FAU - BURKHARDT; BURKHARDT B FAU - SZCZEPANOWSKI *et al.*).

4.2.5 MYC Activity Score in HOVON-84

For the HOVON-84 cohort, we classified 77 cases (44%) as MYC high and 98 (56%) cases as MYC low (Figure 8A).

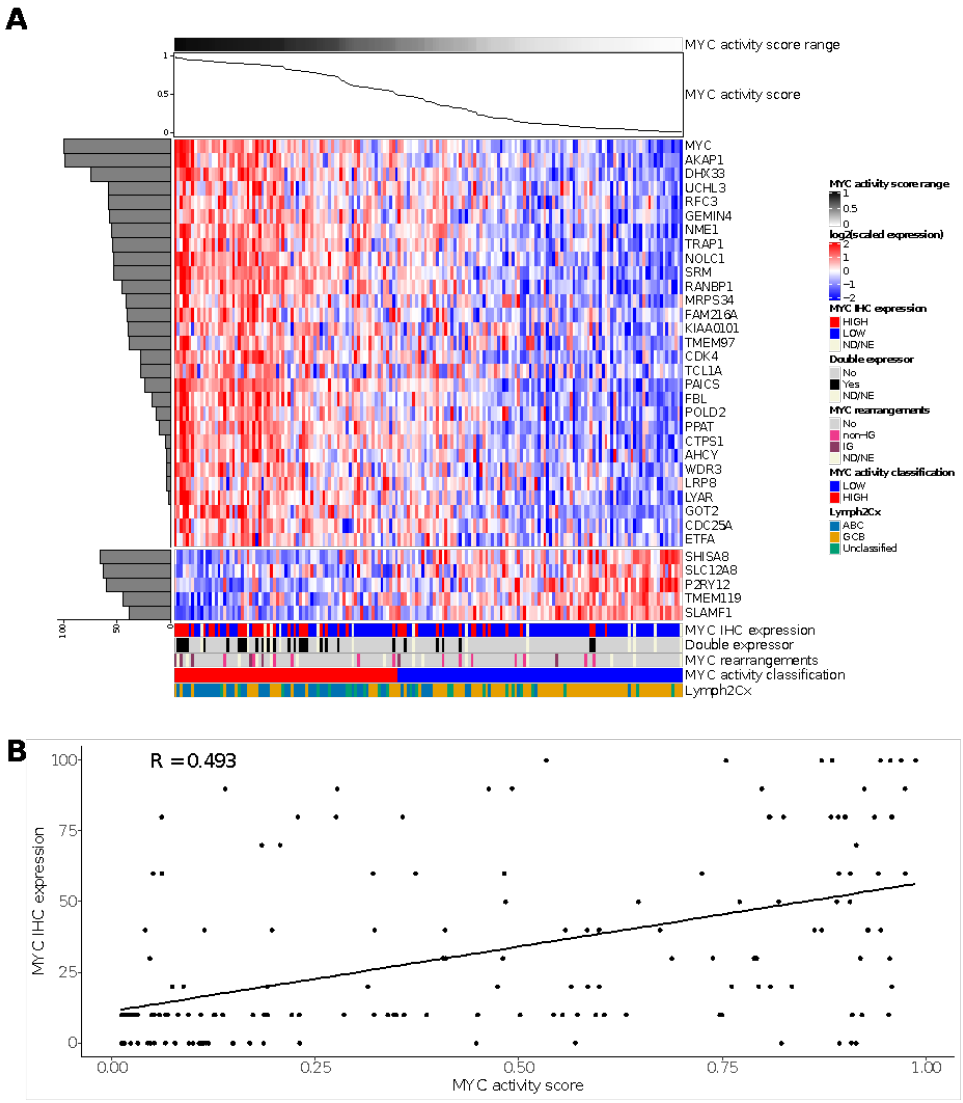

Figure 8. Results of the MYC activity classifier in the HOVON-84 cohort: (A) Heatmap for relative expression of the profiling panel including the relative contribution of each gene to the classifier (horizontal, shaded bar graph on the left) and the MYC activity score for the HOVON-84 cohort (line graph on top of the figure). (B) Spearman's correlation between MYC activity score and MYC IHC expression for the 161 samples of the HOVON-84 cohort. ND, Not Done; NE, Not Evaluable

The sensitivity and specificity values relative to the MYC IHC score based on staining in at least 50% of the tumor cells were 0.65 and 0.65, respectively. The negative and positive predictive values were 0.82 and 0.43, respectively, for the identification of MYC IHC expression (Table 5). A significant correlation (R 0.493; Fisher exact test p = 0.006) was observed for the MYC activity score and the percentage of tumor cells staining

positive for MYC in the HOVON-84 cohort (Figure 8B). The high-activity MYC group was enriched for DE ($p < 0.00001$) and ABC-type ($p < 0.00001$) lymphoma. There was no association between the MYC activity score and HGBCL DH. Thus, the MYC activity score could be validated in the HOVON-84 cohort and showed a clear correlation with DE and ABC-type lymphomas.

4.2.6 Monti Consensus Clustering in HOVON-84

For the HOVON-84 cases, application of the validated algorithms revealed two as the most optimal number of clusters (Figure 9A,B).

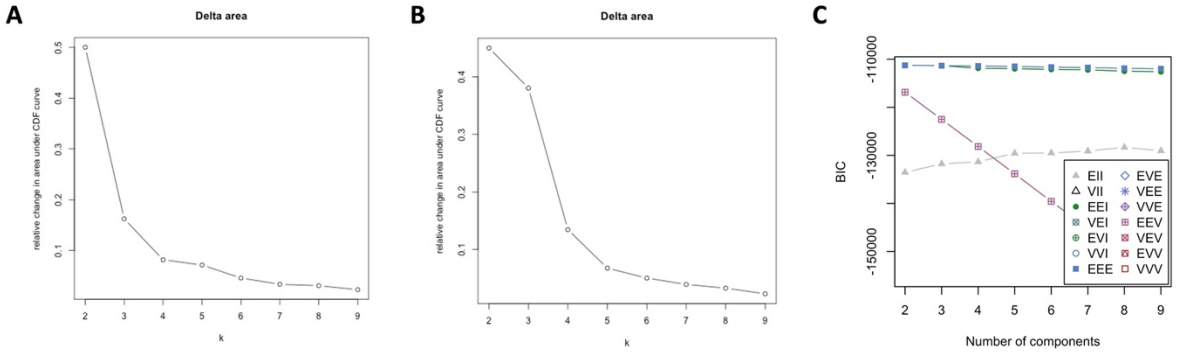

D

	HC - C1	HC – C2	R Total
SOM - C1	43	52	95
SOM - C2	30	50	80
C Total	73	102	175

E

	HC - C1	HC – C2	R Total
PC - C1	95	42	137
PC - C2	0	38	38
C Total	95	80	175

F

	PC - C1	PC – C2	R Total
SOM - C1	59	14	73
SOM- C2	78	24	102
C Total	137	38	175

Figure 9. Identification of consensus clusters in the HOVON-84 cohort using 47 selected genes following the approach as published by Monti. (**a**) Relative change in area under CDF curve for HC algorithm for k from 2 to 9 with 175 samples. (**b**) Relative change in area under CDF curve for SOM algorithm for k from 2 to 9 with 175 samples. (**c**) BIC for PC algorithm for k from 2 to 9 with 175 samples. (**d**) Contingency table between clusters identified by HC and SOM algorithms. (**e**) Contingency table between clusters identified by HC and PC algorithms. (**f**) Contingency table between clusters identified by PC and SOM algorithms. After doing the first step of consensus clustering we tried to re-cluster the non-Host Response subgroup, however the samples didn't differentiate in a new cluster, as in Monti paper.

The meta-consensus clustering exhibited a consistent subgroup for all three algorithms for 67 (38%) HOVON-84 cases. These cases were characterized by two profiles: a larger cluster (43 samples–24%) with high expression of both BCR/proliferation and Oxphos genes (BCR/Proliferation/Oxphos-high cases) and a cluster (24 samples–

14%) characterized by a high expression of HR genes (HR-high cases). Thus, in contrast to the findings of Monti, the non-HR cases were not characterized by a differential expression of BCR/proliferation and Oxphos genes.

Next, we followed the same strategy as reported by Monti to define the most likely cluster for the remaining 108 (62%) HOVON-84 cases. This revealed a consensus BCR/proliferation/Oxphos-high cluster signature for 77 (44%) samples and a consensus HR cluster-signature for 31 (18%) samples. In total 120 (77 + 43) cases were classified as BCR/proliferation/OxPhos-high and 55 (24 + 31) cases (31%) as HR cluster (Figure 10).

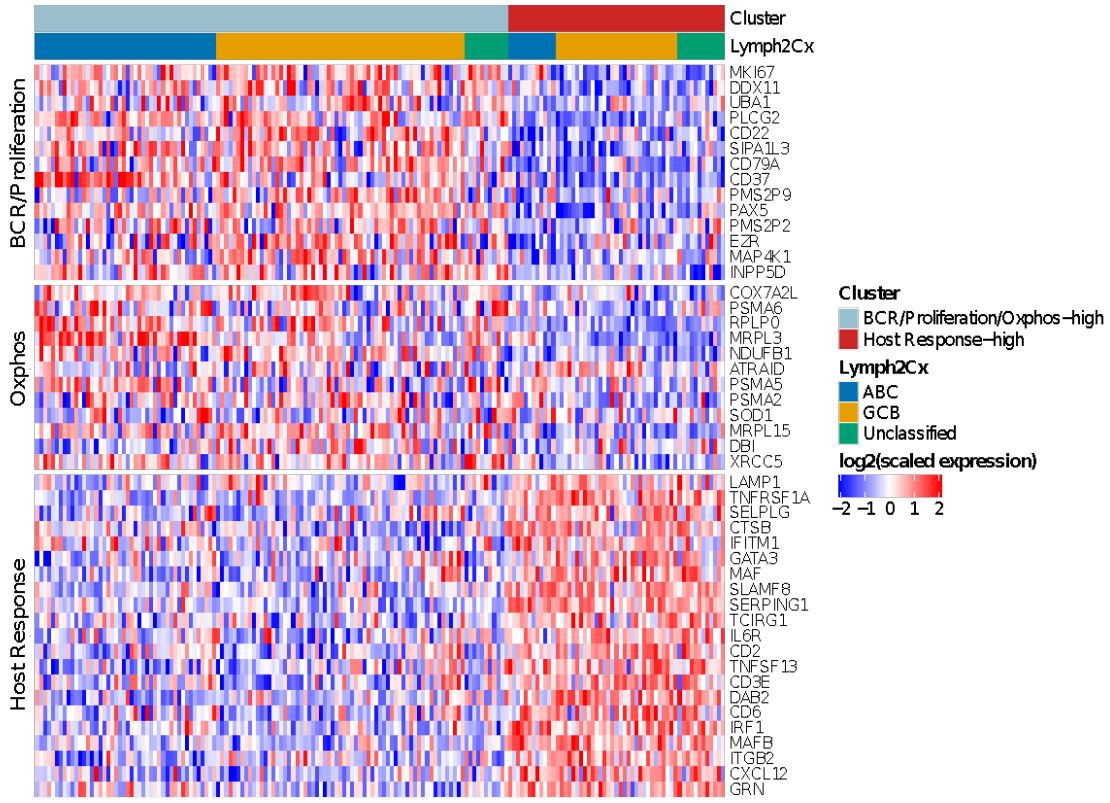

Figure 10. Heatmap showing the relative expression levels of BCR/Proliferation, Host Response (HR) and Oxphos genes used to reproduce the Monti consensus clustering. The HR cluster was validated in 55/175 HOVON-84 cases; the remaining cases showed low expression of HR genes, but no distinct clustering based on BCR/Proliferation and Oxphos genes.

The clusters were distributed across all three COO groups, with an enrichment of BCR/proliferation/Oxphos-high cluster in ABC cases (p = 0.02). In summary, the HR

cluster, but not the BCR/Proliferation and Oxphos clusters could be validated in the HOVON-84 cohort.

4.2.7 Immune-Ratio Classifier

The immune ratio (KEANE; VARI; HERTZBERG; CAO *et al.*, 2015) revealed a ratio under the cut-off for 74 (42%) of the HOVON-84 samples (Figure 11).

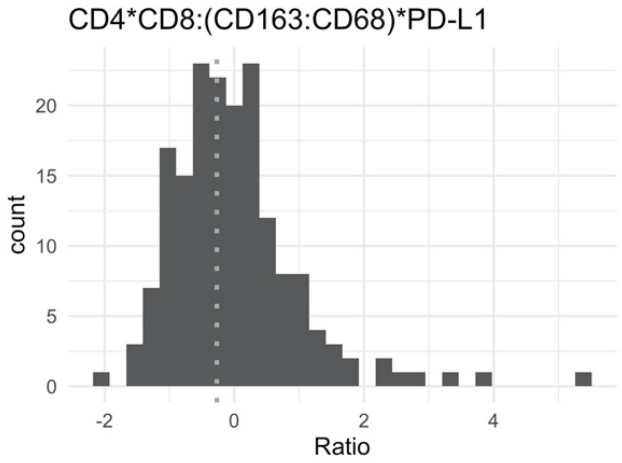

Figure 11. Reproduction of the immune ratio. Distribution of the *CD4*CD8*:(*CD163*:*CD68*)**PD-L1* immuno-ratio for HOVON-84 cohort. The grey line indicates the cut-off (-0.278958829) used to stratify OS in the Keane et al., 2015.

4.2.8 Comparison of the Reproduced GEPs

Next, we compared the four expression signatures to establish a potential overlapping or shared biology. We focused on the overlap among the three larger GEP profiles and separately analyzed a potential overlap with the immune-ratio signature. The mutual impact of the COO, MYC, and the HR group of the Monti consensus clustering signatures, is shown in Figure 12. The overall picture indicated that the three profiles reflect different aspects of lymphoma biology, with no clear overlap. Most ABC cases were characterized by high MYC activity (45/58–77.6%; $p < 0.00001$), whereas the consensus HR-cluster was uncommon (12/58–20% samples) and showed no clear pattern in relation to the MYC signature ($p = 0.44$). The GCB samples largely consisted of MYC-low activity cases (73/94–77.7%; $p < 0.00001$), with in about one third of the

cases a consensus HR-cluster (31/94–33%). The smaller GCB/MYC-high group was enriched for DH (p = 0.019), DE (p = 0.41) and MYC immune positive cases (p = 0.002). About half of the cases in the COO-Unclassified cases were high MYC activity (11/23–48%) and consensus HR cases (12/23–52%). Thus, the MYC and consensus clustering profiles within the COO-Unclassified cases showed an intermediate profile and did not indicate a closer association with either ABC or GCB-type DLBCL

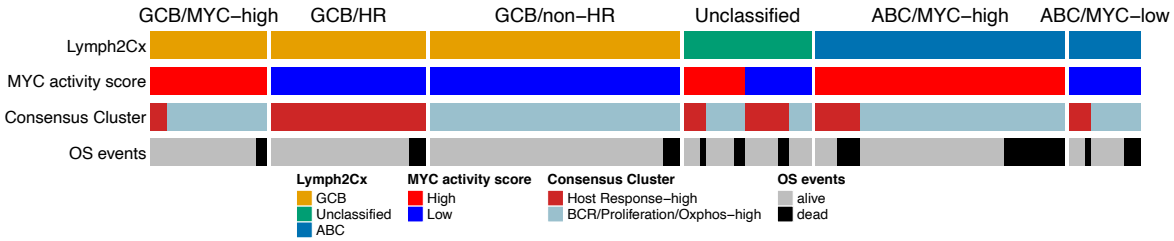

Figure 12. Overlap of the gene expression signatures that were validated in the HOVON-84 cohort. The three signatures show no clear overlap and together are likely to capture different aspects of DLBCL biology. OS events were observed in each of the six clusters, with a slight enrichment in the ABC/MYC-high group.

The high immune-ratio subgroup was associated with the HR consensus cluster (OR = 2.82; p = 0.003) and with the high MYC activity cluster (OR = 0.387; p = 0.003) while no association was found with the COO classifier (Figure 13).

Figure 13. Overlap of Immune ratio, Lymph2CX and Consensus Clusters signatures in the HOVON-84 cohort. There is an association between high Immune ratio and high Host Response. No association with Lymph2Cx was found.

We evaluated the correlation of MHC-II IHC with the different gene signatures as proposed by Ennishi et al. 2020. We did not identify an association of MHC-II-IHC high and HLA-II-IHC with COO, MYC activity score, Monti consensus clustering, and immune-ratio signatures.

4.2.9 Prognostic Impact of Validated Signatures

Consistent with previous publications, poor aaIPI, which does not consider age, advanced age (>60 years), the COO ABC-type, and the high MYC activity score were significantly associated with poor five-years OS in a univariate analysis (Figure 14A–C, 15A and Figure 16A). The HR cluster of the Monti consensus clustering had no impact on survival consistent with the original report (Figure 14D). In contrast to the original paper, we could not validate the prognostic relevance of the immune-ratio classifier (Hazard ratio 1.6; p = 0.2) (Figure 14E). Other MYC molecular features known to impact patient's survival based on the literature such as high MYC IHC expression and DE and DH events had no impact on five-years OS (Figure 15B-D).

Multivariate analysis including the four variables significant in the univariate analysis, i.e., aaIPI, age, GCB versus ABC, and MYC activity score showed that only the COO ABC-type remained prognostic (Hazard ratio 3.06; p = 0.023) (Figure 16B).

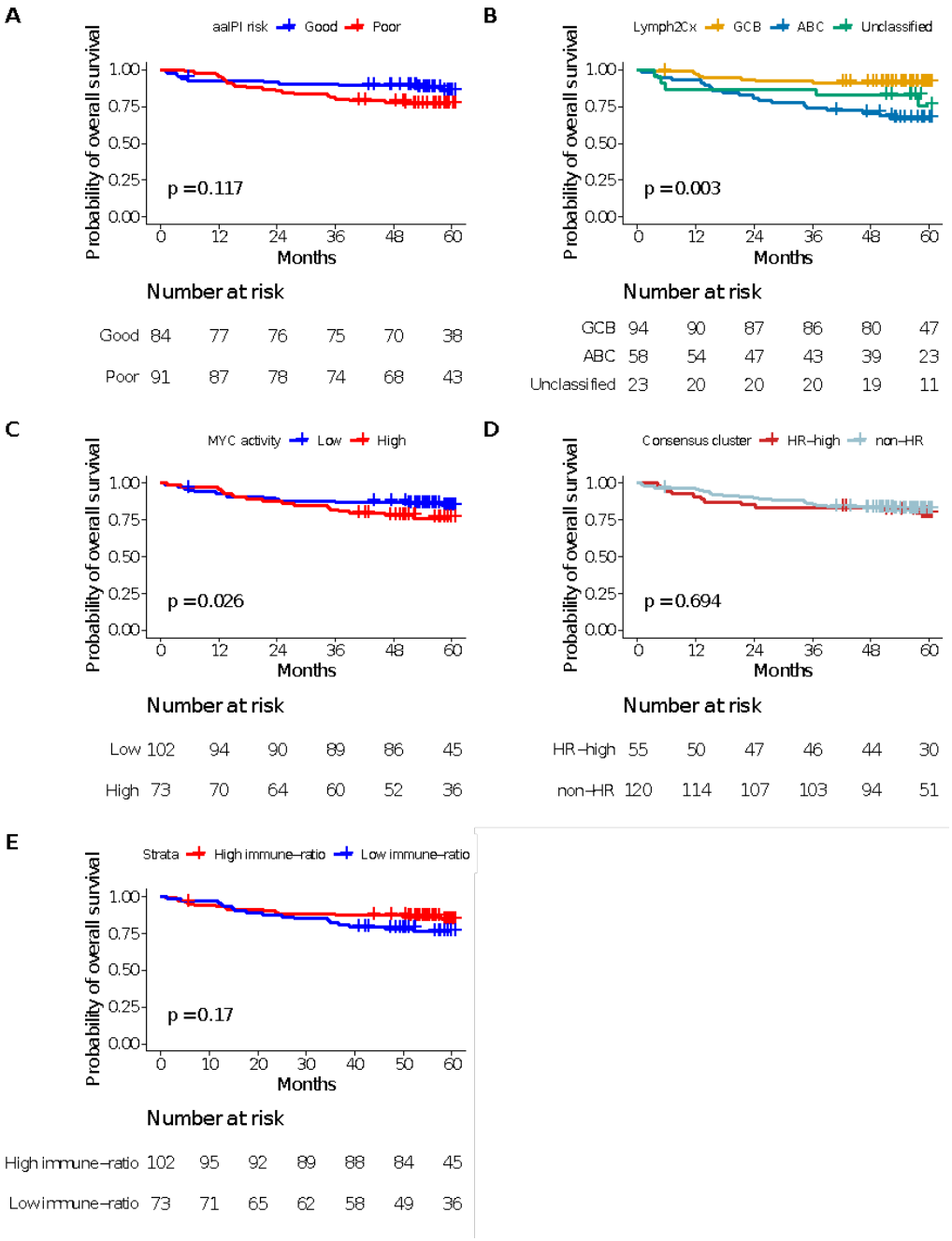

Figure 14. Kaplan–Meier curves showing overall survival of 175 patients from the HOVON-84 cohort: According to (A) the aaIPI, (B) the COO classification defined by the Lymph2Cx algorithm, (C) the Monti consensus clusters, (D) the MYC activity classifier, (E) the immune-ratio subgroups.

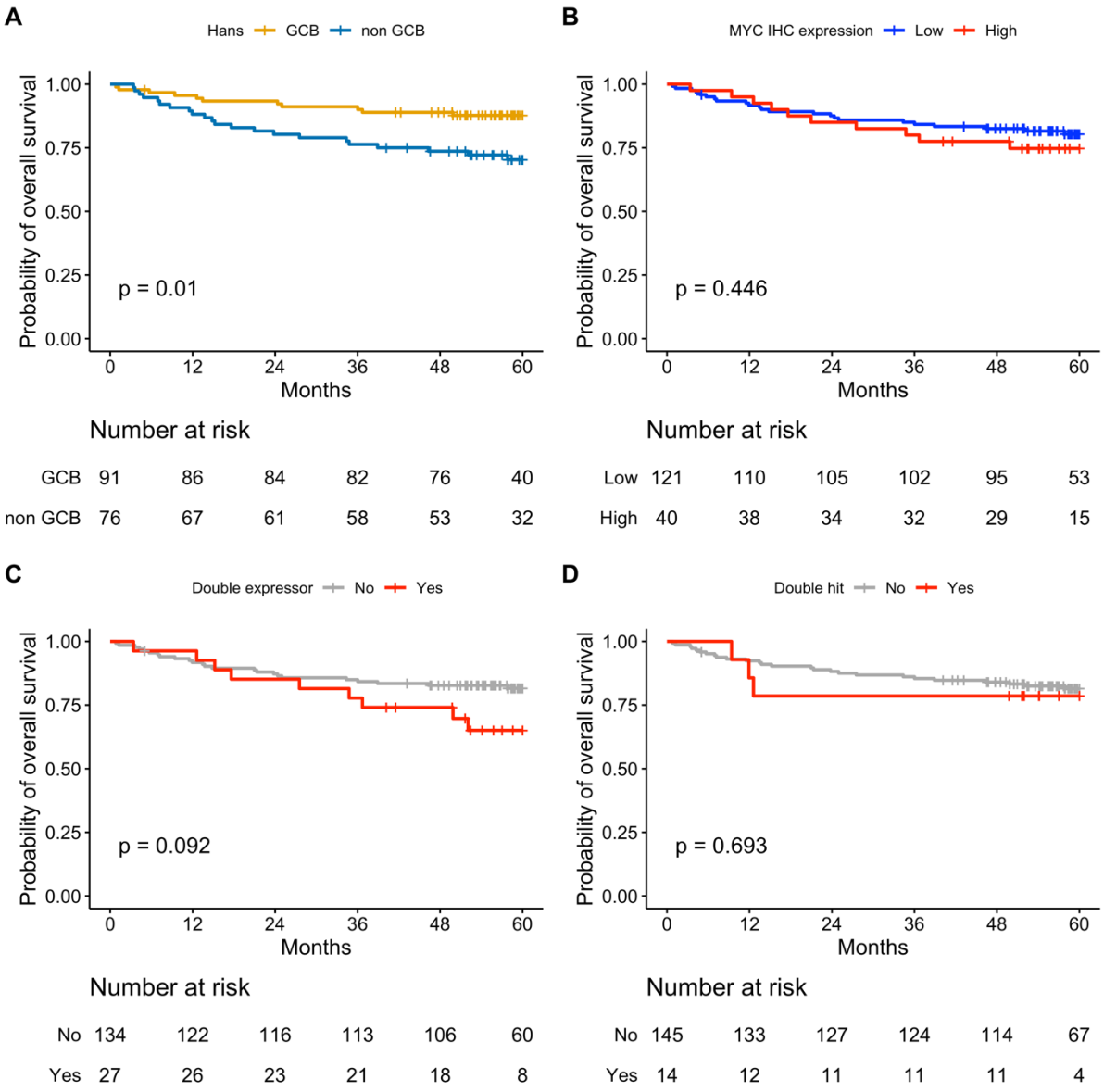

Figure 15. Kaplan Meier curves for overall survival of the HOVON-84 cohort for (**a**) the COO classification defined by Hans. (**b**) the MYC IHC expression low (<50%) and high (>50%) subgroups. (**c**) Double expressor lymphoma. (**d**) Double-hit lymphoma.

A

Univariate analysis

Group	Class	Number of patients	Mean hazard ratio	P–value
aaIPI	Good (reference)	84	–	
	Poor	91	2.1	0.043
Age	< 60 (reference)	59	–	
	>= 60	116	3.3	0.014
Lymph2Cx	GCB (reference)	94	–	
	ABC	58	3.6	0.001
	Unclassified	23	2.1	0.165
MYC activity score	Low (reference)	86	–	
	High	66	2.1	0.026
Consensus cluster	non–HR (reference)	120	–	
	HR – high	55	0.86	0.681
Immune–ratio	Low (reference)	73	–	
	High	102	1.6	0.13

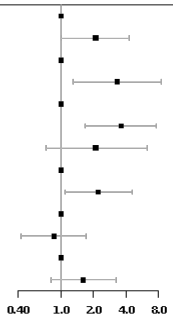

B

Multivariate analysis

Group	Class	Number of patients	Mean hazard ratio	P–value
aaIPI	Good (reference)	69	–	
	Poor	83	2.28	0.064
Age	< 60 (reference)	51	–	
	>= 60	101	4.43	0.049
Lymph2Cx	GCB (reference)	94	–	
	ABC	58	3.06	0.023
MYC activity score	Low (reference)	86	–	
	High	66	0.95	0.917

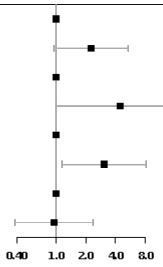

Figure 16. Five-year OS of HOVON-84 patients: (A) Forest plot with the univariate effect of the clinical variables and GEP signatures. (B) Forest plot with the multivariate effect of clinical variables and GEP signatures. In this cohort, only the COO as defined by the Lymph2Cx remains signific

4.3 Discussion

In this NanoString-based GEP-profiling study we used a selected set of genes to validate previously published signatures. With this limited set of genes, we were able to faithfully reproduce the classifications of the original MYC activity score and Monti consensus clustering algorithms. Besides the COO, we also reproduced the HR cluster of the Monti consensus clustering and the MYC activity signature in the well-defined HOVON84 study population. We were not able to reproduce the BCR or Oxphos signatures of the Monti consensus clustering. In contrast to the original study, we did not observe a significant difference in survival for the immune-response ratio (KEANE; VARI; HERTZBERG; CAO *et al.*, 2015).

Although COO is well established, its prognostic value has been disputed (STAIGER; ZIEPERT; HORN; SCOTT *et al.*, 2017). The poor survival as observed for ABC type DLBCL has been used as a starting point for the design of several clinical trials.

Combination of lenalidomide and ibrutinib in relapsed DLBCL showed efficacy particularly in patients with Hans-based non-GCB type DLBCL, supporting clinical relevance of the COO concept (GOY; RAMCHANDREN; GHOSH; MUNOZ *et al.*, 2019). Molecular subclassification with or without considering the COO might be used for the design of more focused clinical trials to improve the outcome of specific DLBCL subgroups (CHAPUY; STEWART; DUNFORD; KIM *et al.*, 2018; ENNISHI; HSI; STEIDL; SCOTT ; SCHMITZ; WRIGHT; HUANG; JOHNSON *et al.*, 2018).

There are several ways to categorize DLBCL cases based on MYC status: i.e., DH (FISH), DE (IHC), and GEP classifiers. The more recently published DH GEP signature enables identification of cases with cryptic MYC rearrangements (ENNISHI; JIANG; BOYLE; COLLINGE *et al.*, 2019). The biological rationale underlying the MYC activity GEP signatures is evident, since this enables capturing of the indirect activity of MYC; although, implementation of such a profile in clinical practice warrants further development. We were able to reproduce the Carey MYC classifier, but the impact of the genes was different from the original paper. A possible explanation for this difference might be that our cohort includes cases with the entire spectrum of percentage positive cells, whereas the training set from Carey has been selected for cases with more extreme IHC-based MYC scores. The differences in the spectrum of MYC scores possibly explains the weaker correlation and lower positive predictive value for identifying HGBCL-DH in the HOVON-84 samples. The high MYC activity group showed a poor outcome, while DH cases had no impact on OS, probably because we observed a limited number of events in the HOVON-84 cohort of patients with a HGBCL-DH. Nevertheless, comparison of different algorithms is needed to select the best algorithm for clinical application.

The HR cluster was the most eminent profile identified by Monti et al. and highlights the TME as a defining feature. HR cases had increased expression of genes associated with T-cell-mediated immune responses, the classical complement pathway, coregulated inflammatory mediators, and connective tissue components. A micro-environment-based GE profiling described by Lenz et al. (LENZ; WRIGHT; DAVE; XIAO *et al.*, 2008) (macrophage 1 (M1) and macrophage 2 signatures (M2)) showed a clear distribution among the COO subgroups. Although we did not include the genes to validate the M1 and M2 signatures, the inflammatory response described by Monti et al. is characterized

by and recapitulates this profile. More recently, a novel interest for microenvironment-based GEP using CIBERSORT (CHEN; KHODADOUST; LIU; NEWMAN *et al.*, 2018) or single-cell RNA-seq analysis has arisen. The clinical value of the HR signature might become more important with the rise of a whole new range of therapies, including chimeric antigen receptor T cells (CAR T-cells) and bispecific monoclonal antibodies, where the nature of the microenvironment is likely to be important for a durable clinical response (QIN; JOHNSTONE; BATUREVYCH; HAUSE *et al.*, 2020).

Recently, three additional signatures associated with MYC and TME were reported (CIAVARELLA; VEGLIANTE; FABBRI; DE SUMMA *et al.*, 2018; ENNISHI; JIANG; BOYLE; COLLINGE *et al.*, 2019; STAIGER; ALTENBUCHINGER; ZIEPERT; KOHLER *et al.*, 2020). However, the limited overlap with our gene panel precluded validation of these signatures. Most likely, part of these studies basically looks at similar underlying biology, including two different MYC classifiers but using a different set of genes (CAREY; GUSENLEITNER; CHAPUY; KOVACH *et al.*, 2015; ENNISHI; JIANG; BOYLE; COLLINGE *et al.*, 2019). There was no evident overlap among the COO, HR, and MYC activity subgroups, emphasizing that each classifier captures a different aspect of the biological heterogeneous panorama. In a recent review, a reclassification of DLBCL based on molecular genetics and gene expression profiling was proposed by Ennishi et al.. We now show experimental evidence supporting their proposed subgrouping, with GCB-type DLBCL samples being split in three subgroups as high MYC activity non-HR cases and low MYC activity score splitting in either HR or non-HR cases. Similarly, ABC DLBCL were mainly characterized by high MYC activity scores. However, we did not find any associations with MHC-II expression in the HOVOV-84 cohort. So, our data mostly support the newly proposed classification by Ennishi et al. and emphasizes the importance of biology-driven molecular subgroups.

Profiling of a dedicated subset of genes has become feasible using the Nanostring gene expression system even on FFPE tissue samples containing poor quality RNA. We show a reliable classification of DLBCL cases with multiple gene expression signatures even when using a limited set of genes. Further validation studies are required to link the established signatures to more recently published GEP and mutational signatures and elucidate the complete spectrum of the very heterogenous group of DLBCL. Beyond the

biological relevance, COO and MYC activity gene expression signatures had an impact on survival. This highlights the potential of combining different classifiers to improve the identification of high-risk cases and emphasizes the need to integrate these signatures in future clinical trials. The limited gene set required to generate the signatures in combination with the freely available algorithms enables a strait forward and cost-effective implementation. Moreover, combining multiple GEP may lead to improved stratification of patients into specific molecular subgroups that may be sensitive to specific targeted therapeutics.

5 CONCLUSIONS

We have extensively characterized CD4+CD26- T cells in the TME of cHL. These T cells are antigen experienced and probably originate from memory Treg cells. They are enriched for exhaustion associated transcription factors TOX and TOX2, which also induce expression of immune checkpoints. Targeting of TOX and TOX2 might reverse T cell exhaustion and thereby provides an interesting opportunity for immunotherapy.

We showed that COO, MYC activity score, and the HR cluster of the Monti consensus clustering were reproduced in the HOVON-84 cohort of DLBCL patients. These three signatures identify distinct subgroups based on different aspects of DLBCL biology, emphasizing that each classifier captures distinct molecular profiles, offering a framework for clinical trials. More comparative studies with gene expression profiles need to be done to enable a further integration and to help develop new taxonomy systems for clinical utility.

6 REFERENCES

AGRAWAL, V.; SU, M.; HUANG, Y.; HSING, M. *et al.* Computer-Aided Discovery of Small Molecule Inhibitors of Thymocyte Selection-Associated High Mobility Group Box Protein (TOX) as Potential Therapeutics for Cutaneous T-Cell Lymphomas. **Molecules**, 24, n. 19, Sep 24 2019.

ALFEI, F.; KANEV, K.; HOFMANN, M.; WU, M. *et al.* TOX reinforces the phenotype and longevity of exhausted T cells in chronic viral infection. **Nature**, 571, n. 7764, p. 265-269, Jul 2019.

ALIAHMAD, P.; KAYE, J. Development of all CD4 T lineages requires nuclear factor TOX. **J Exp Med**, 205, n. 1, p. 245-256, Jan 21 2008.

ALIZADEH, A. A.; EISEN, M. B.; DAVIS, R. E.; MA, C. *et al.* Distinct types of diffuse large B-cell lymphoma identified by gene expression profiling. **Nature**, 403, n. 6769, p. 503-511, Feb 3 2000.

AOKI, T.; CHONG, L. C.; TAKATA, K.; MILNE, K. *et al.* Single-Cell Transcriptome Analysis Reveals Disease-Defining T-cell Subsets in the Tumor Microenvironment of Classic Hodgkin Lymphoma. **Cancer Discov**, 10, n. 3, p. 406-421, Mar 2020.

BEJARANO, L.; JORDÃO, M. J. C.; JOYCE, J. A. Therapeutic Targeting of the Tumor Microenvironment. **Cancer Discov**, 11, n. 4, p. 933-959, Apr 2021.

BRÖCKELMANN, P. J.; GOERGEN, H.; KELLER, U.; MEISSNER, J. *et al.* Efficacy of Nivolumab and AVD in Early-Stage Unfavorable Classic Hodgkin Lymphoma: The Randomized Phase 2 German Hodgkin Study Group NIVAHL Trial. **JAMA Oncol**, 6, n. 6, p. 872-880, Jun 1 2020.

CADER, F. Z.; HU, X.; GOH, W. L.; WIENAND, K. *et al.* A peripheral immune signature of responsiveness to PD-1 blockade in patients with classical Hodgkin lymphoma. **Nat Med**, 26, n. 9, p. 1468-1479, Sep 2020.

CADER, F. Z.; SCHACKMANN, R. C. J.; HU, X.; WIENAND, K. *et al.* Mass cytometry of Hodgkin lymphoma reveals a CD4(+) regulatory T-cell-rich and exhausted T-effector microenvironment. **Blood**, 132, n. 8, p. 825-836, Aug 23 2018.

CÂNCER, I. N. D. **Estimativa 2020**. 2020. Disponível em: https://www.inca.gov.br/estimativa/estado-capital/brasil.

CAREY, C. D.; GUSENLEITNER, D.; CHAPUY, B.; KOVACH, A. E. *et al.* Molecular classification of MYC-driven B-cell lymphomas by targeted gene expression profiling of fixed biopsy specimens. **J Mol Diagn**, 17, n. 1, p. 19-30, Jan 2015.

CAREY, C. D.; GUSENLEITNER, D.; LIPSCHITZ, M.; ROEMER, M. G. M. *et al.* Topological analysis reveals a PD-L1-associated microenvironmental niche for Reed-Sternberg cells in Hodgkin lymphoma. **Blood**, 130, n. 22, p. 2420-2430, Nov 30 2017.

CASAN, J. M.; BARRACLOUGH, A.; SHORTT, J.; HAWKES, E. A. Dose-adjusted EPOCH-R therapy in MYC-rearranged diffuse large B-cell lymphoma: not yet the standard of care. **Lancet Haematol**, 6, n. 3, p. e119, Mar 2019.

CASEY, S. C.; AMEDEI, A.; AQUILANO, K.; AZMI, A. S. *et al.* Cancer prevention and therapy through the modulation of the tumor microenvironment. **Seminars in Cancer Biology**, 35, p. S199-S223, 2015/12/01/ 2015.

CHAMULEAU, M. E. D.; BURGGRAAFF, C. N.; NIJLAND, M.; BAKUNINA, K. *et al.* Treatment of patients with MYC rearrangement positive large B-cell lymphoma with R-CHOP plus lenalidomide: results of a multicenter HOVON phase II trial. **Haematologica**, Dec 19 2019.

CHAN, F. C.; TELENIUS, A.; HEALY, S.; BEN-NERIAH, S. *et al.* An RCOR1 loss-associated gene expression signature identifies a prognostically significant DLBCL subgroup. **Blood**, 125, n. 6, p. 959-966, Feb 5 2015.

CHAPUY, B.; STEWART, C.; DUNFORD, A. J.; KIM, J. *et al.* Molecular subtypes of diffuse large B cell lymphoma are associated with distinct pathogenic mechanisms and outcomes. **Nat Med**, 24, n. 5, p. 679-690, May 2018.

CHEN, B.; KHODADOUST, M. S.; LIU, C. L.; NEWMAN, A. M. *et al.* Profiling Tumor Infiltrating Immune Cells with CIBERSORT. **Methods Mol Biol**, 1711, p. 243-259, 2018.

CIAVARELLA, S.; VEGLIANTE, M. C.; FABBRI, M.; DE SUMMA, S. *et al.* Dissection of DLBCL microenvironment provides a gene expression-based predictor of survival applicable to formalin-fixed paraffin-embedded tissue. **Ann Oncol**, 29, n. 12, p. 2363-2370, Dec 1 2018.

ENNISHI, D.; HSI, E. D.; STEIDL, C.; SCOTT, D. W. Toward a New Molecular Taxonomy of Diffuse Large B-cell Lymphoma. n. 2159-8290 (Electronic).

ENNISHI, D.; JIANG, A.; BOYLE, M.; COLLINGE, B. *et al.* Double-Hit Gene Expression Signature Defines a Distinct Subgroup of Germinal Center B-Cell-Like Diffuse Large B-Cell Lymphoma. **J Clin Oncol**, 37, n. 3, p. 190-201, Jan 20 2019.

FERRARINI, I.; RIGO, A.; ZAMÒ, A.; VINANTE, F. Classical Hodgkin lymphoma cells may promote an IL-17-enriched microenvironment. **Leuk Lymphoma**, 60, n. 14, p. 3395-3405, Dec 2019.

FLEISCHER, B. CD26: a surface protease involved in T-cell activation. **Immunol Today**, 15, n. 4, p. 180-184, Apr 1994.

FROMM, J. R.; KUSSICK, S. J.; WOOD, B. L. Identification and purification of classical Hodgkin cells from lymph nodes by flow cytometry and flow cytometric cell sorting. **Am J Clin Pathol**, 126, n. 5, p. 764-780, Nov 2006.

GEVREY, M.; DIMOPOULOS, I.; LEK, S. Review and comparison of methods to study the contribution of variables in artificial neural network models. **Ecological Modelling**, 160, n. 3, p. 249-264, 2003/02/15/ 2003.

GOY, A.; RAMCHANDREN, R.; GHOSH, N.; MUNOZ, J. *et al.* Ibrutinib plus lenalidomide and rituximab has promising activity in relapsed/refractory non-germinal center B-cell-like DLBCL. **Blood**, 134, n. 13, p. 1024-1036, Sep 26 2019.

HANS, C. P.; WEISENBURGER, D. D.; GREINER, T. C.; GASCOYNE, R. D. *et al.* Confirmation of the molecular classification of diffuse large B-cell lymphoma by immunohistochemistry using a tissue microarray. **Blood**, 103, n. 1, p. 275-282, Jan 1 2004.

HOLLANDER, P.; ROSTGAARD, K.; SMEDBY, K. E.; MOLIN, D. *et al.* An anergic immune signature in the tumor microenvironment of classical Hodgkin lymphoma is associated with inferior outcome. **Eur J Haematol**, 100, n. 1, p. 88-97, Jan 2018.

HU, S.; XU-MONETTE, Z. Y.; TZANKOV, A.; GREEN, T. *et al.* MYC/BCL2 protein coexpression contributes to the inferior survival of activated B-cell subtype of diffuse large B-cell lymphoma and demonstrates high-risk gene expression signatures: a report from The International DLBCL Rituximab-CHOP Consortium Program. **Blood**, 121, n. 20, p. 4021-4031; quiz 4250, May 16 2013.

HUANG, S.; LIANG, C.; ZHAO, Y.; DENG, T. *et al.* Increased TOX expression concurrent with PD-1, Tim-3, and CD244 in T cells from patients with non-Hodgkin lymphoma. **Asia Pac J Clin Oncol**, 18, n. 1, p. 143-149, Feb 2022.

HUI, L.; CHEN, Y. Tumor microenvironment: Sanctuary of the devil. **Cancer Lett**, 368, n. 1, p. 7-13, Nov 1 2015.

IAFC, R. **Global Cancer Observatory: Non-Hodgkin lymphoma**. 2018. Disponível em: https://gco.iarc.fr/today/data/factsheets/cancers/34-Non-hodgkin-lymphoma-fact-sheet.pdf. Acesso em: 18/03/2020
.

IELLEM, A.; MARIANI, M.; LANG, R.; RECALDE, H. *et al.* Unique chemotactic response profile and specific expression of chemokine receptors CCR4 and CCR8 by CD4(+)CD25(+) regulatory T cells. **J Exp Med**, 194, n. 6, p. 847-853, Sep 17 2001.

ISHIDA, T.; ISHII, T.; INAGAKI, A.; YANO, H. *et al.* Specific recruitment of CC chemokine receptor 4-positive regulatory T cells in Hodgkin lymphoma fosters immune privilege. **Cancer Res**, 66, n. 11, p. 5716-5722, Jun 1 2006.

JUNTTILA, M. R.; DE SAUVAGE, F. J. Influence of tumour micro-environment heterogeneity on therapeutic response. **Nature**, 501, n. 7467, p. 346-354, Sep 19 2013.

KEANE, C.; VARI, F.; HERTZBERG, M.; CAO, K. A. *et al.* Ratios of T-cell immune effectors and checkpoint molecules as prognostic biomarkers in diffuse large B-cell lymphoma: a population-based study. **Lancet Haematol**, 2, n. 10, p. e445-455, Oct 2015.

KIM, D.; PAGGI, J. M.; PARK, C.; BENNETT, C. *et al.* Graph-based genome alignment and genotyping with HISAT2 and HISAT-genotype. **Nat Biotechnol**, 37, n. 8, p. 907-915, Aug 2019.

KIM, K.; PARK, S.; PARK, S. Y.; KIM, G. *et al.* Single-cell transcriptome analysis reveals TOX as a promoting factor for T cell exhaustion and a predictor for anti-PD-1 responses in human cancer. **Genome Med**, 12, n. 1, p. 22, Feb 28 2020.

KLAPPER, W.; KREUZ M FAU - KOHLER, C. W.; KOHLER CW FAU - BURKHARDT, B.; BURKHARDT B FAU - SZCZEPANOWSKI, M. *et al.* Patient age at diagnosis is associated with the molecular characteristics of diffuse large B-cell lymphoma. n. 1528-0020 (Electronic).

KLEMANN, C.; WAGNER, L.; STEPHAN, M.; VON HÖRSTEN, S. Cut to the chase: a review of CD26/dipeptidyl peptidase-4's (DPP4) entanglement in the immune system. **Clin Exp Immunol**, 185, n. 1, p. 1-21, Jul 2016.

KUHN, M. Building Predictive Models in R Using the caret Package. **Journal of Statistical Software**, 28, n. 5, 2008.

LACY, S. E.; BARRANS, S. L.; BEER, P. A.; PAINTER, D. *et al.* Targeted sequencing in DLBCL, molecular subtypes, and outcomes: a Haematological Malignancy Research Network report. **Blood**, 135, n. 20, p. 1759-1771, May 14 2020.

LENZ, G.; WRIGHT, G.; DAVE, S. S.; XIAO, W. *et al.* Stromal gene signatures in large-B-cell lymphomas. **N Engl J Med**, 359, n. 22, p. 2313-2323, Nov 27 2008.

LEONARD, J. P.; KOLIBABA, K. S.; REEVES, J. A.; TULPULE, A. *et al.* Randomized Phase II Study of R-CHOP With or Without Bortezomib in Previously Untreated Patients With Non-Germinal Center B-Cell-Like Diffuse Large B-Cell Lymphoma. **J Clin Oncol**, 35, n. 31, p. 3538-3546, Nov 1 2017.

LI, C.; KIM, S. W.; RAI, D.; BOLLA, A. R. *et al.* Copy number abnormalities, MYC activity, and the genetic fingerprint of normal B cells mechanistically define the microRNA profile of diffuse large B-cell lymphoma. **Blood**, 113, n. 26, p. 6681-6690, Jun 25 2009.

LIANG, C.; HUANG, S.; ZHAO, Y.; CHEN, S. *et al.* TOX as a potential target for immunotherapy in lymphocytic malignancies. **Biomark Res**, 9, n. 1, p. 20, Mar 20 2021.

LIU, Y.; SATTARZADEH, A.; DIEPSTRA, A.; VISSER, L. *et al.* The microenvironment in classical Hodgkin lymphoma: an actively shaped and essential tumor component. **Semin Cancer Biol**, 24, p. 15-22, Feb 2014.

LOVE, M. I.; HUBER, W.; ANDERS, S. Moderated estimation of fold change and dispersion for RNA-seq data with DESeq2. **Genome Biol**, 15, n. 12, p. 550, 2014.

LUGTENBURG, P. J.; BROWN, P. d. N.; HOLT, B. v. d.; D'AMORE, F. A. *et al.* Rituximab-CHOP with early rituximab intensification for diffuse large B-cell lymphoma: a randomized phase 3 trial of the HOVON and the Nordic Lymphoma Group (HOVON-84). **Journal of Clinical Oncology**, 2020.

MA, Y.; VISSER, L.; BLOKZIJL, T.; HARMS, G. *et al.* The CD4+CD26- T-cell population in classical Hodgkin's lymphoma displays a distinctive regulatory T-cell profile. **Lab Invest**, 88, n. 5, p. 482-490, May 2008.

MAESTRE, L.; GARCÍA-GARCÍA, J. F.; JIMÉNEZ, S.; REYES-GARCÍA, A. I. *et al.* High-mobility group box (TOX) antibody a useful tool for the identification of B and T cell subpopulations. **PLoS One**, 15, n. 2, p. e0229743, 2020.

MASQUÉ-SOLER, N.; SZCZEPANOWSKI, M.; KOHLER, C. W.; SPANG, R. *et al.* Molecular classification of mature aggressive B-cell lymphoma using digital multiplexed gene expression on formalin-fixed paraffin-embedded biopsy specimens. **Blood**, 122, n. 11, p. 1985-1986, Sep 12 2013.

MENDEVILLE, M.; ROEMER, M. G. M.; VAN DEN HOUT, M.; LOS-DE VRIES, G. T. *et al.* Aggressive genomic features in clinically indolent primary HHV8-negative effusion-based lymphoma. **Blood**, 133, n. 4, p. 377-380, Jan 24 2019.

MERRYMAN, R. W.; ARMAND, P.; WRIGHT, K. T.; RODIG, S. J. Checkpoint blockade in Hodgkin and non-Hodgkin lymphoma. **Blood Adv**, 1, n. 26, p. 2643-2654, Dec 12 2017.

MONTI, S.; SAVAGE, K. J.; KUTOK, J. L.; FEUERHAKE, F. *et al.* Molecular profiling of diffuse large B-cell lymphoma identifies robust subtypes including one characterized by host inflammatory response. **Blood**, 105, n. 5, p. 1851-1861, Mar 1 2005.

NAGASAKI, J.; TOGASHI, Y.; SUGAWARA, T.; ITAMI, M. *et al.* The critical role of CD4+ T cells in PD-1 blockade against MHC-II-expressing tumors such as classic Hodgkin lymphoma. **Blood Adv**, 4, n. 17, p. 4069-4082, Sep 8 2020.

NIENS, M.; VISSER, L.; NOLTE, I. M.; VAN DER STEEGE, G. *et al.* Serum chemokine levels in Hodgkin lymphoma patients: highly increased levels of CCL17 and CCL22. **Br J Haematol**, 140, n. 5, p. 527-536, Mar 2008.

NIJLAND, M.; VEENSTRA, R. N.; VISSER, L.; XU, C. *et al.* HLA dependent immune escape mechanisms in B-cell lymphomas: Implications for immune checkpoint inhibitor therapy? n. 2162-4011 (Print).

PATEL, S. S.; WEIRATHER, J. L.; LIPSCHITZ, M.; LAKO, A. *et al.* The microenvironmental niche in classic Hodgkin lymphoma is enriched for CTLA-4-positive T cells that are PD-1-negative. **Blood**, 134, n. 23, p. 2059-2069, Dec 5 2019.

POPPEMA, S. The nature of the lymphocytes surrounding Reed-Sternberg cells in nodular lymphocyte predominance and in other types of Hodgkin's disease. **Am J Pathol**, 135, n. 2, p. 351-357, Aug 1989.

POPPEMA, S. Immunology of Hodgkin's disease. **Baillieres Clin Haematol**, 9, n. 3, p. 447-457, Sep 1996.

POPPEMA, S.; BHAN, A. K.; REINHERZ, E. L.; POSNER, M. R. *et al.* In situ immunologic characterization of cellular constituents in lymph nodes and spleens involved by Hodgkin's disease. **Blood**, 59, n. 2, p. 226-232, Feb 1982.

QIN, J. S.; JOHNSTONE, T. G.; BATUREVYCH, A.; HAUSE, R. J. *et al.* Antitumor Potency of an Anti-CD19 Chimeric Antigen Receptor T-Cell Therapy, Lisocabtagene Maraleucel in Combination With Ibrutinib or Acalabrutinib. **J Immunother**, 43, n. 4, p. 107-120, May 2020.

RAMCHANDREN, R.; DOMINGO-DOMÈNECH, E.; RUEDA, A.; TRNĚNÝ, M. *et al.* Nivolumab for Newly Diagnosed Advanced-Stage Classic Hodgkin Lymphoma: Safety and Efficacy in the Phase II CheckMate 205 Study. **J Clin Oncol**, 37, n. 23, p. 1997-2007, Aug 10 2019.

REDDY, A.; ZHANG, J.; DAVIS, N. S.; MOFFITT, A. B. *et al.* Genetic and Functional Drivers of Diffuse Large B Cell Lymphoma. **Cell**, 171, n. 2, p. 481-494.e415, Oct 5 2017.

ROEMER, M. G. M.; REDD, R. A.; CADER, F. Z.; PAK, C. J. *et al.* Major Histocompatibility Complex Class II and Programmed Death Ligand 1 Expression Predict Outcome After Programmed Death 1 Blockade in Classic Hodgkin Lymphoma. **J Clin Oncol**, 36, n. 10, p. 942-950, Apr 1 2018.

ROIDER, T.; SEUFERT, J.; UVAROVSKII, A.; FRAUHAMMER, F. *et al.* Dissecting intratumour heterogeneity of nodal B-cell lymphomas at the transcriptional, genetic and drug-response levels. **Nat Cell Biol**, 22, n. 7, p. 896-906, Jul 2020.

ROSENWALD, A.; BENS, S.; ADVANI, R.; BARRANS, S. *et al.* Prognostic Significance of MYC Rearrangement and Translocation Partner in Diffuse Large B-Cell Lymphoma: A Study by the Lunenburg Lymphoma Biomarker Consortium. **J Clin Oncol**, 37, n. 35, p. 3359-3368, Dec 10 2019.

SALLES, G.; DE JONG, D.; XIE, W.; ROSENWALD, A. *et al.* Prognostic significance of immunohistochemical biomarkers in diffuse large B-cell lymphoma: a study from the Lunenburg Lymphoma Biomarker Consortium. **Blood**, 117, n. 26, p. 7070-7078, Jun 30 2011.

SCHMIEDEL, B. J.; SINGH, D.; MADRIGAL, A.; VALDOVINO-GONZALEZ, A. G. *et al.* Impact of Genetic Polymorphisms on Human Immune Cell Gene Expression. n. 1097-4172 (Electronic).

SCHMIEDEL, B. J.; SINGH, D.; MADRIGAL, A.; VALDOVINO-GONZALEZ, A. G. *et al.* Impact of Genetic Polymorphisms on Human Immune Cell Gene Expression. **Cell**, 175, n. 6, p. 1701-1715.e1716, Nov 29 2018.

SCHMITZ, R.; WRIGHT, G. W.; HUANG, D. W.; JOHNSON, C. A. *et al.* Genetics and Pathogenesis of Diffuse Large B-Cell Lymphoma. **N Engl J Med**, 378, n. 15, p. 1396-1407, Apr 12 2018.

SCOTT, A. C.; DÜNDAR, F.; ZUMBO, P.; CHANDRAN, S. S. *et al.* TOX is a critical regulator of tumour-specific T cell differentiation. **Nature**, 571, n. 7764, p. 270-274, Jul 2019.

SCOTT, D. W.; GASCOYNE, R. D. The tumour microenvironment in B cell lymphomas. **Nat Rev Cancer**, 14, n. 8, p. 517-534, Aug 2014.

SCOTT, D. W.; WRIGHT, G. W.; WILLIAMS, P. M.; LIH, C. J. *et al.* Determining cell-of-origin subtypes of diffuse large B-cell lymphoma using gene expression in formalin-fixed paraffin-embedded tissue. **Blood**, 123, n. 8, p. 1214-1217, Feb 20 2014.

SCRUCCA, L.; FOP, M.; MURPHY, T. B.; RAFTERY, A. E. mclust 5: Clustering, Classification and Density Estimation Using Gaussian Finite Mixture Models. n. 2073-4859 (Print).

SEHN, L. H.; BERRY, B.; CHHANABHAI, M.; FITZGERALD, C. *et al.* The revised International Prognostic Index (R-IPI) is a better predictor of outcome than the standard IPI for patients with diffuse large B-cell lymphoma treated with R-CHOP. **Blood**, 109, n. 5, p. 1857-1861, Mar 1 2007.

SEHN, L. H.; SALLES, G. Diffuse Large B-Cell Lymphoma. **N Engl J Med**, 384, n. 9, p. 842-858, Mar 4 2021.

SEO, H. A.-O.; CHEN, J.; GONZÁLEZ-AVALOS, E.; SAMANIEGO-CASTRUITA, D. *et al.* TOX and TOX2 transcription factors cooperate with NR4A transcription factors to impose CD8(+) T cell exhaustion. n. 1091-6490 (Electronic).

SHIPP, M. A.; ROSS, K. N.; TAMAYO, P.; WENG, A. P. *et al.* Diffuse large B-cell lymphoma outcome prediction by gene-expression profiling and supervised machine learning. **Nat Med**, 8, n. 1, p. 68-74, Jan 2002.

STAIGER, A. M.; ALTENBUCHINGER, M.; ZIEPERT, M.; KOHLER, C. *et al.* A novel lymphoma-associated macrophage interaction signature (LAMIS) provides robust risk prognostication in diffuse large B-cell lymphoma clinical trial cohorts of the DSHNHL. **Leukemia**, 34, n. 2, p. 543-552, Feb 2020.

STAIGER, A. M.; ZIEPERT, M.; HORN, H.; SCOTT, D. W. *et al.* Clinical Impact of the Cell-of-Origin Classification and the MYC/ BCL2 Dual Expresser Status in Diffuse Large B-Cell Lymphoma Treated Within Prospective Clinical Trials of the German High-Grade Non-Hodgkin's Lymphoma Study Group. **J Clin Oncol**, 35, n. 22, p. 2515-2526, Aug 1 2017.

STUART, A. E.; WILLIAMS, A. R.; HABESHAW, J. A. Rosetting and other reactions of the Reed-Sternberg cell. **J Pathol**, 122, n. 2, p. 81-90, Jun 1977.

SWERDLOW, S.; CAMPO, E.; HARRIS, N. WHO Classification of Tumours of Haematopoietic and Lymphoid Tissues. Lyon, France: World Health Organization 2017.

SWERDLOW, S. H.; CAMPO, E.; PILERI, S. A.; HARRIS, N. L. *et al.* The 2016 revision of the World Health Organization classification of lymphoid neoplasms. **Blood**, 127, n. 20, p. 2375-2390, May 19 2016.

TANAKA, T.; CAMERINI, D.; SEED, B.; TORIMOTO, Y. *et al.* Cloning and functional expression of the T cell activation antigen CD26. **J Immunol**, 149, n. 2, p. 481-486, Jul 15 1992.

TEAM, R. C. **R: A Language and Environment for Statistical Computing**. R Foundation for Statistical Computing, 2019.

VELDMAN, J.; VISSER, L.; HUBERTS-KREGEL, M.; MULLER, N. *et al.* Rosetting T cells in Hodgkin lymphoma are activated by immunological synapse components HLA class II and CD58. **Blood**, 136, n. 21, p. 2437-2441, Nov 19 2020.

VELDMAN-JONES, M. H.; BRANT, R.; ROONEY, C.; GEH, C. *et al.* Evaluating Robustness and Sensitivity of the NanoString Technologies nCounter Platform to Enable Multiplexed Gene Expression Analysis of Clinical Samples. n. 1538-7445 (Electronic).

VITOLO, U.; WITZIG, T. E.; GASCOYNE, R. D.; SCOTT, D. W. *et al.* ROBUST: First report of phase III randomized study of lenalidomide/R-CHOP (R2-CHOP) vs placebo/R-CHOP in previously untreated ABC-type diffuse large B-cell lymphoma. **Hematological Oncology**, 37, n. S2, p. 36-37, 2019.

VOLTIN, C. A.; METTLER, J.; VAN HEEK, L.; GOERGEN, H. *et al.* Early Response to First-Line Anti-PD-1 Treatment in Hodgkin Lymphoma: A PET-Based Analysis from the Prospective, Randomized Phase II NIVAHL Trial. **Clin Cancer Res**, 27, n. 2, p. 402-407, Jan 15 2021.

VONG, Q. P.; LEUNG, W. H.; HOUSTON, J.; LI, Y. *et al.* TOX2 regulates human natural killer cell development by controlling T-BET expression. **Blood**, 124, n. 26, p. 3905-3913, Dec 18 2014.

WAGGOTT, D.; CHU K FAU - YIN, S.; YIN S FAU - WOUTERS, B. G.; WOUTERS BG FAU - LIU, F.-F. *et al.* NanoStringNorm: an extensible R package for the pre-processing of NanoString mRNA and miRNA data. n. 1367-4811 (Electronic).

WANG, L.; DING, K.; ZHENG, C.; XIAO, H. *et al.* Detachable Nanoparticle-Enhanced Chemoimmunotherapy Based on Precise Killing of Tumor Seeds and Normalizing the Growing Soil Strategy. **Nano Lett**, 20, n. 9, p. 6272-6280, Sep 9 2020.

WANG, X.; HE, Q.; SHEN, H.; XIA, A. *et al.* TOX promotes the exhaustion of antitumor CD8(+) T cells by preventing PD1 degradation in hepatocellular carcinoma. **J Hepatol**, 71, n. 4, p. 731-741, Oct 2019.

WEHRENS, R.; KRUISSELBRINK, J. Flexible Self-Organizing Maps in kohonen 3.0. **Journal of Statistical Software**, 87, n. 7, p. 1 - 18, 11/12 2018.

WILKERSON, M. D.; HAYES, D. N. ConsensusClusterPlus: a class discovery tool with confidence assessments and item tracking. n. 1367-4811 (Electronic).

XU, W.; ZHAO, X.; WANG, X.; FENG, H. *et al.* The Transcription Factor Tox2 Drives T Follicular Helper Cell Development via Regulating Chromatin Accessibility. **Immunity**, 51, n. 5, p. 826-839.e825, Nov 19 2019.

YAO, C.; SUN, H. W.; LACEY, N. E.; JI, Y. *et al.* Single-cell RNA-seq reveals TOX as a key regulator of CD8(+) T cell persistence in chronic infection. **Nat Immunol**, 20, n. 7, p. 890-901, Jul 2019.

YOON, N.; AHN, S.; YONG YOO, H.; JIN KIM, S. *et al.* Cell-of-origin of diffuse large B-cell lymphomas determined by the Lymph2Cx assay: better prognostic indicator than Hans algorithm. **Oncotarget**, 8, n. 13, p. 22014-22022, Mar 28 2017.

YOUNES, A.; SEHN, L. H.; JOHNSON, P.; ZINZANI, P. L. *et al.* Randomized Phase III Trial of Ibrutinib and Rituximab Plus Cyclophosphamide, Doxorubicin, Vincristine, and Prednisone in Non-Germinal Center B-Cell Diffuse Large B-Cell Lymphoma. **J Clin Oncol**, 37, n. 15, p. 1285-1295, May 20 2019.

YU, X.; LI, Z. TOX gene: a novel target for human cancer gene therapy. **Am J Cancer Res**, 5, n. 12, p. 3516-3524, 2015.